UNIVERSITY OF CALIFORNIA,
IRVINE

Behavior of Typical Skewed and Curved Bridges in Extreme Seismic Events

THESIS

Submitted in partial satisfaction of the requirements
for the degree of

MASTER OF SCIENCE

In Civil Engineering

by

Pere Pla-Junca

Thesis Committee:
Professor Farzin Zareian, Chair
Professor Ayman Mosallam
Pofessor Masanobu Shinozuka

2010

DEDICATION

To

Rosa Lecina Fabrés

TABLE OF CONTENTS

LIST OF FIGURES

LIST OF TABLES

ACKNOWLEDGEMENTS

I was awarded with a Balsells Fellowship in 2009 to pursue my master's studies in University of California, Irvine. I would like to express my sincere gratitude to Mr. Pere Balsells and all the institutions involved in this fellowship for their financial support during the last year. In addition, this study is based on work supported by the PEER Lifeline Program under Grant No. UCB-PEER 00006938. This financial support is gratefully acknowledged.

I would like to thank the committee chair, Professor Farzin Zareian, for his worthy advice and guidance in all those aspects related to my academic and professional careers, for having always been respectful toward my interests as student and as an engineer, and for the great knowledge he has transferred to me.

I would also like to express my gratitude to Peyman Kaviani for letting me use his three proficient skewed bridge models for this study and having significantly contributed to my current knowledge of bridge modeling. I also thank you to Professor Curt B. Haselton, from California State University, Chico, and Thomas Shantz, Senior Research Engineer from Caltrans Division of Research and Innovation. Both are part of the team involved in this project. Professor Curt B. Haselton has been responsible for selecting and modifying sets of ground motions according to the procedures proposed by the GMSM methods selected, and Thomas Shantz has been responsible for modeling the foundations of the bridges considered in this research project.

I am also grateful to my friends in Barcelona, who equipped me with the laptop I am writing these words of gratitude with, and those I met here for having enriched my experience in Irvine.

I definitely thank you my parents, my older sister and my younger brother for their always unconditional help and enormous love.

I would like to finish expressing my extreme and most sincere gratitude to Rosa Lecina Fabrés. She is constantly motivating and encouraging me to face new challenges and keep working hard to accomplish my professional goals. Her wholehearted support, patience and comprehension are extraordinary, and her love is immense. All my work has been done thanks to her.

ABSTRACT OF THE THESIS

Behavior of Typical Skewed and Curved Bridges in Extreme Seismic Events

By

Pere Pla-Junca

Master of Structural Engineering

University of California, Irvine, 2010

Professor Farzin Zareian, Chair

This study is on evaluation of two GMSM methods for estimation of bridge response parameters during seismic excitation. The main focus is on understanding the behavior and proper modeling of the structures used to conduct such evaluation.

A total of six bridges, three skewed and three curved bridges, design by the California Transportation Department, Caltrans, and located in Orange and Los Angeles counties are considered. They are modeled using OpenSees (McKenna et al. 2000) open-source structural analysis platform. The selected GMSM methods are labeled as $Sa(T_1)$ scaling (where T_1 is the fundamental period of the bridge under consideration) and Conditional Mean Spectrum (CMS) scaling. For each method, several sets of scaled ground motions are generated. These sets of records are applied to the bridges and the respective responses are analyzed.

Curved bridges present numerical instabilities when using force-based elements to model their columns. Displacement-based elements are used instead. Pushover analysis of the bridges every 5º can be used to determine their strongest and weakest directions. For curved bridges, these are those defined by an axis tangent to the arc described by the

deck in its middle point and the corresponding perpendicular axis, respectively. For skewed bridges, the transverse is the strongest direction, and the longitudinal the weakest. A method for computing the plastic hinge length of a column is proposed. Finally, the structural responses obtained using $Sa(T_1)$ scaling and CMS scaling methods do not show any clear trend.

CHAPTER 1

INTRODUCTION

1.1. MOTIVATION AND BACKGROUND

Acceptance of nonlinear response history analysis (NRHA) has increased over the last years, especially for seismic assessment of existing structures and for new designs created based on the principles of performance-based engineering. The increasing use of such analysis in structural engineering demands to improve its accuracy in estimation of structures response. Progress is constantly being made to address this critical aspect. However, new methodologies enhancing the accuracy usually penalize the time needed to perform the analysis. On the contrary, those procedures aiming for a reduction of the time analysis generally imply certain loss of accuracy in the results.

Multiple NRHA are generally required for understanding a structure's behavior during expected seismic excitations. The number of NRHA is definitely limited by the computational effort they require, but also by the ability of the ground motion records finally selected and scaled to faithfully represent the seismicity of the area where the structure is located. The average structural response predicted from these multiple NRHA, or the probability distribution of the same, is very sensitive to these ground motion records.

The present thesis shows the first part of a larger project with an objective to evaluate different ground motion selection and modification (GMSM) methods currently available in order to be able to define practical guidelines for their use in bridge

structures. Such evaluation has already been done for buildings by the PEER GMSM Working Group (C. B. Haselton et al., 2009). A part from being different type of structures considered herein, another difference with respect to the work of this group is that its evaluation was based on unidirectional ground motion studies, while bidirectional ground motion studies are also conducted in this case, due to the fact that bridges clearly have two principal directions with differing responses, identified as longitudinal and transverse directions.

The methodology that this group followed to evaluate the GMSM methods is also followed in this study. The first step is to select a series of methods commonly used by engineers and scientist for ground motion selection and scaling. The following step is to use these methods to select and modify sets of ground motion records. The sets resulting from the selection and modification process are then applied to a group of structures representative of the target type of structures, and their structural responses are predicted. The next step is to generate what is called "point of comparison" (POC) or high-end prediction. Given a structure, the POC is defined as its estimated true response, i.e., the best prediction of the value of those engineering demand parameters (EDPs) selected to describe its structural response. Finally, the GMSM methods are evaluated. The evaluation consists in comparing the results of each method to those of the others and also to the POC, which is assumed to be the exact solution. In this study, the POC is not computed thus the comparison to this high-end prediction is not conducted. However, the procedure that must be followed to compute the POC is exposed in Chapter 4.

The GMSM methods evaluated in the present thesis are the $Sa(T_1)$ scaling method ($Sa(T_1)$ refers to the spectral acceleration value at the fundamental period of the structure)

and the CMS scaling method (J. W. Baker, 2010) (CMS stands for conditional mean spectrum). They are explained in detail in Chapter 2. From each method, sets of modified ground motion records are generated. Special attention is given to the CMS scaling method, because its purpose is to select and modify records such that each of them meets a target averaged value of $Sa(T_1)$ and, at the same time, the total set matches the variability of the target response spectrum.

Models of various real structures are needed to test the GMSM methods selected. They must be a manageable number of structures and, at the same time, representative of as many typologies as possible, in order to make the future practical guidelines derived from the present study applicable to a wide range of cases. Six bridges are modeled. They are divided in two groups: a first group of one straight bridge and two skewed bridges, and a second group consisting of three curved bridges. All the structures have been designed by California Transportation Department, Caltrans, and they all meet the criteria for being classified as ordinary standard bridges. Although these are commonly used structures, there are significant lacks of knowledge of their real response under seismic loads, and there are important uncertainties regarding their modeling. These set of structures is considered to be representative enough of the typologies more frequently used nowadays.

All the structures are modeled with OpenSees open-source structural analysis platform (McKenna et al. 2000). A detailed description of the modeling is presented in Chapter 3, along with four side studies. The first side study aims for determining the proper type of finite elements needed to model the columns of the bridges .The second side study is to determine the bridges' strongest and weakest directions by utilizing

pushover analysis in several directions. The third side study clarifies an uncertainty related to how OpenSees manages the input ground motion records. The last side study proposes a method to determine the plastic hinge length of the columns.

The EDPs selected to describe the structural behavior of the bridges are the maximum displacement of the column bents and the maximum displacement of the abutments. Both EDPs determine the capacity of the bridges to withstand seismic loads, but the first EDP, in terms of the strength of the columns, which are the elements allowed to behave inelastic, while the second EDP, in terms of unseating of the deck.

Chapter 4 evaluates Sa(T1) scaling and CMS scaling methods followed by Chapter 5 discussion on modeling and application of these selected GMSM methods.

1.2. OBJECTIVES

This thesis presents the first part of a larger project aiming towards evaluation of various GMSM methods for estimation of bridge response in seismic excitation.

The goals of this research are three-fold. First, is to study the behavior of skewed and curved bridges by means of the observation of the performance of the models of these structures under the sets of ground motion records selected and modified by the GMSM methods considered. Second objective is to determine the proper model for bridges that leads to a reliable structural response, or, at least, identify those modeling aspects that have a strong influence in the results. Last objective is to evaluate the $Sa(T_1)$ scaling and CMS scaling GMSM methods.

CHAPTER 2

GROUND MOTION SELECTION AND MODIFICATION (GMSM) METHODS USED IN THIS STUDY

2.1. INTRODUCTION

The present chapter describes those ground motion selection and modification (GMSM) methods selected for this study. As commented in the previous chapter, the research project conducted by GMSM Working Group (C. B. Haselton et al., 2009), in which many GMSM methods were evaluated in order to predict median interstory drift response of buildings, is considered the departure point toward similar research projects but for many other engineering problems, such as bridges, thus it is taken as the point of reference to articulate this study.

A part from being different type of structures analyzed herein from those considered in the reference research project in question, there is another important difference between them: while only unidirectional ground motion studies were conducted in such research project, also bidirectional ground motion studies are conducted in this case. Deciding to perform bidirectional analysis was due to the fact that bridges have a clearly different behavior in longitudinal and transverse directions. In order to develop useful guidelines for selecting and modifying ground motions for their use in bridge dynamic analysis, it is essential to take both directions into consideration.

It is important to remark that the GMSM methods that are referred to here are those consisting in selecting recorded ground motions and possibly scaling their amplitudes. Methods that use spectrum compatible ground motions (i.e., modification of

the frequency content of a ground motion) and methods that simulate ground motions are not considered.

The following definition of possible objectives of GMSM methods and the description of the groups in which they are divided has been extracted from the aforementioned reference project.

2.2. OBJECTIVES OF GMSM METHODS

The objective of a GMSM method is the main purpose of the nonlinear response history analysis being directed making use of the ground motions selected and modified by the GMSM method. Different methods can have different objectives. The following are the objectives in question:

- Objective 1. The first objective is to predict the probability distribution of structural response for an earthquake of a given magnitude (M) and source-to-site distance (R).
- Objective 2. The second objective is to predict the median structural response for an earthquake of a given M and R, i.e., a given earthquake scenario.
- Objective 3. Similar to the first objective, the third objective is to predict the probability distribution of structural response but, in this case, for a ground motion scenario described by the spectral acceleration value at the fundamental period of the structure ($Sa(T_1)$), M, and R. Therefore it is necessary to have certain knowledge of the structure, i.e., its fundamental period T_1.

- Objective 4. The last objective is to predict the median structural response, similar to Objective 2, but, as in the previous objective, for a ground motion scenario defined by a given $Sa(T_1)$, M, and R.

2.3. GMSM METHODS

Two types of methods are selected to scale and modify ground motions. They meet Objective 3 or 4, and they are described below.

2.3.1. Group I Methods ($Sa(T_1)$)

The Group I, or $Sa(T_1)$, methods select ground motions from earthquakes of M and R as close as possible to those of the scenario of interest. Different methods from Group I may consider different earthquake, site, and ground motion parameters. After applying the selection criteria, if the number of ground motions selected is larger than the target number, these methods select from them randomly. But if the selection criteria result in too few ground motions, the criteria are relaxed.

Once the ground motions are selected, each of them is scaled in amplitude such that their $Sa(T_1)$ value is equal to the scenario $Sa(T_1)$ value. The scaling factor applied to all the ground motion acceleration values is equal to the ratio between the scenario $Sa(T_1)$ value and the $Sa(T_1)$ value of the un-scaled ground motion.

Group I GMSM methods target Objective 3, which is to predict the probability distribution of structural response for a ground motion scenario described by a given $Sa(T_1)$, M, and R.

2.3.2. Group II Methods (CMS)

The Group II, or CMS, methods select ground motions whose response spectra, applying simple amplitude scaling of each ground motion if needed, are as close as possible to the target conditional mean spectrum (CMS) (J. W. Baker, 2010). The CMS represents the expected response spectrum for the defined ground motion scenario, and it is calculated from a target $Sa(T_1)$ value at a single period and the associated M and R values.

Not only the spectral shape can be considered to select ground motions with this methods, but also other earthquake, site, and ground motion parameters. Once the ground motions are selected they are modified by simple amplitude scaling.

Unlike Group I methods, Group II methods aim for Objective 4, because they predict the median structural response for a ground motion scenario defined by a given $Sa(T_1)$, M, and R.

2.3.3. GMS Methods Selected

One method of each group is selected and different sets of ground motions are generated. A description of the procedure followed by these GMSM methods finally selected and the sets of ground motions derived from them is next. These methods are $Sa(T_1)$ scaling method and CMS scaling method.

The selection and modification of ground motions according to these two methods have been done by C. B. Haselton.

2.3.3.1. $Sa(T_1)$ Scaling Method

The procedure followed by this method to select and scale ground motions does not take the shape nor the variability of the target response spectrum into consideration, but only the target $Sa(T_1)$. According to N. Shome (C. B. Haselton et al., 2009) the steps in which $Sa(T_1)$ scaling method is divided are:

- Step 1. Determine an M-R-S-F (magnitude, source-to-site distance, site classification, and type of faulting, respectively) bin of ground motions being consistent with the given ground motion scenario.
- Step 2. Select a target number of ground motions randomly from the bin. They should be selected from different earthquakes to capture the inter-event variability of response for a given $Sa(T_1)$.
- Step 3. Scale the ground motions to the target $Sa(T_1)$. In the case of a given M, R, S, and F only, the target $Sa(T_1)$ is the median from a ground motion prediction equation, i.e., an attenuation relationship. The target $Sa(T_1)$ value can also be determined from a Probabilistic Seismic Hazard Analysis (PSHA), but significantly more input information is needed in this case. For this study, as explained in Chapter 4, the target $Sa(T_1)$ is the median value determined using Campbell and Bozorgnia 2008 attenuation model (K. W. Campbell and Y. Bozorgnia, 2007), plus one and a half times the standard deviation value given by the same attenuation model for T_1.

In this case, the M-R-S-F bin is the M 7.0 set defined in Chapter 4, which consists of one hundred and seventeen ground motions. From this M 7.0 set, forty-two pairs of records that verify the following selection criteria have been selected randomly:

- < <
- km < km
- m s
- Lowest usable frequency of 0.25 Hz

R is the source-to-site distance. The restraint for $V_{S,30}$ corresponds to soils classes from A to D. These selection criteria are consistent with the target ground motion scenario. The fourth criterion seeks for assuring that all ground motions loose frequency content in the high period range. As the structures go into nonlinear action, their period elongates. If there is no restraint in the lowest usable frequency, the selected motions will have variable upper excitation period range, and it may happen that some structures get action in those elongated periods, while some others do not. The purpose of this project is to evaluate two GMSM methods in order to be able to develop practical guidelines for their use in a future. This evaluation is based on the comparison between the response of the structures subjected to different sets of ground motions selected and modified by the selected GMSM methods. Therefore it is needed to work with records that produce responses that can be compared to each other. Knowing the consequences of having records with variable upper excitation period range commented above, fixing a lowest usable frequency is required to ensure having comparable responses.

From the original set of forty-two un-scaled pairs of records, two subsets are generated, one subset for performing unidirectional ground motion studies and another subset for performing bidirectional ground motion studies. Given a pair of records, each of them has an associated response spectrum related to a certain critical damping value, which is equal to 5% in this study. From these response spectra, $Sa(T_1)_i^{C1}$ and $Sa(T_1)_i^{C2}$

are determined, where the subscript i refers to the i^{th} pair, and the superscripts C1 and C2 denote component 1 and 2, respectively. The unidirectional subset consists of forty-two pairs of records whose components are scaled as follows:

- Scale factor for component 1 ($SF_i^{C1}|_{Sa}$):

$$F_{i}^{C}{}_{a} = \frac{a^{t}}{a^{C}_{i}} \tag{2.1}$$

  where $Sa(T_1)^{(t)}$ is the target $Sa(T_1)$, the subscript Sa refers to the $Sa(T_1)$ scaling method, and the rest of the parameters has already been indicated previously.

- Scale factor for component 2 ($SF_i^{C2}|_{Sa}$):

$$F_{i}^{C}{}_{a} = \frac{a^{t}}{a^{C}_{i}} \tag{2.2}$$

  where all the parameters have already been indicated previously.

Each scaled component is applied in the longitudinal direction of the bridge, thus this subset is equivalent to a subset of eighty-four records differently scaled to match the target $Sa(T_1)$ value.

The bidirectional subset consists of the same forty-two pairs of records but each pair is applied to the bridge simultaneously, the first component in the longitudinal direction and the second component in the transverse direction, and the scaling factor is the same for both of them and equal to the ratio between the target $Sa(T_1)$ and the geometric mean of $Sa(T_1)_i^{C1}$ and $Sa(T_1)_i^{C2}$, i.e.:

$$F_{i\,a} = \frac{a^{t}}{\sqrt{a_{i}^{C}\, a_{i}^{C}}} \tag{2.3}$$

where $SF^{i}|_{Sa}$ is the scaling factor, and the rest of the parameters has already been indicated previously.

$Sa(T_1)^{(t)}$ is determined as described in Chapter 4, when defining the target ground motion scenario.

2.3.3.2. CMS Scaling Method

This method selects ground motions such that their response spectrum matches the CMS for the period of interest, which is the fundamental period of the bridge under consideration, and in a way that the set of records finally selected also meets the variability of the CMS. For this purpose, the ground motion selection algorithm for matching a target response spectrum mean and variance proposed by N. Jayaram et al. (2010) is used. Before applying this algorithm, it is necessary to obtain the CMS. The next is a description of the procedure to compute it.

The CMS is a response spectrum associated with a target Sa value at a single period and consistent with the PSHA. According to J. W. Baker (2010) the steps for computing this response spectrum are:

- Step 1. Determine the target Sa at a given period of interest T* (Sa(T*)), and the associated and epsilon ε

  In this case, T* is equal to the T_1 of the bridge considered. Like the previous method, the target Sa(T*) is computed as the median value of Sa at T*

predicted by Campbell and Bozorgnia 2008 attenuation model, plus one and a half times the value of the standard deviation predicted by the same attenuation model for * he and ε are those of the target ground motion scenario defined in Chapter 4, i.e., 7.0, 15 km and 1.5, respectively. Given an arbitrary period, T, ε is defined as the number of standard deviations by which the natural logarithm of Sa(T) (lnSa(T)) differs from the predicted mean of lnSa(T) for a given M and R. ε can be written as follows:

$$\varepsilon = \frac{\ln a \quad \ln a}{\ln a} \tag{2.4}$$

where $\mu_{\ln Sa}$ and $_{\ln Sa}(T)$ are the predicted mean and standard deviation of lnSa(T), respectively, computed from a certain ground motion model. As mentioned above, the ground motion model selected for this study is the Campbell and Bozorgnia 2008 attenuation model.

From equation 2.4, the target Sa(T*) can be expressed as:

$$a \quad * = e^{\varepsilon \quad * \quad \ln a \quad * \quad \ln a \quad *} \tag{2.5}$$

where all the parameters have already been indicated previously.

- Step 2. Compute the mean and standard deviation of the response spectrum at other periods, given M and R.

  The mean and the standard deviation referred to in this step are the quantities presented in Step 1, i.e., $\mu_{\ln Sa}$ and $_{\ln Sa}(T)$, respectively. In this step, these values are computed at periods included in the range of periods of interest. The recommendations given by J. W. Baker (2010) are (1) to select a

range of periods going from $0.2T_1$ to $2T_1$, and (2) to consider at least fifty values per order of magnitude of periods within the range finally selected, thus within the recommended range, at least fifty periods should be considered.

- Step 3. Compute ε at other periods given ε *

  he third step consists in computing conditional mean ε values for those periods, T_i, considered within the range of interest ($\mu_{\varepsilon\ i\ \varepsilon\ *}$). $\mu_{\varepsilon\ i\ \varepsilon\ *}$ can be calculated as the product of ε * and the correlation coefficient between the ε values at the two periods ρ_{i,T^*}), i.e.:

$$\varepsilon_{i\ \varepsilon\ *} = \rho_{i} * \varepsilon *$$

(2.6)

According to J. W. Baker (2010), the following simple predictive equation, valid for periods between and sec onds can be used to obtained ρ_{i,T^*}):

$$\rho_{\min\ \max} = \cos\left(- \left(\quad {}_{\min<} \quad \ln\frac{\min}{}\right)\ln\frac{\max}{\min}\right)$$

(2.7)

where $I_{(Tmin<0.189)}$ is an indicator function equal to 1 if Tmin < 0.189 sec, and equal to 0 otherwise, and T_{min} and T_{max} are the smaller and larger of the two periods of interest.

- Step 4. Compute Conditional Mean Spectrum.

  At each period of interest, T_i, the corresponding spectral accelerations that define the CMS can be computed combining equations 2.4 and 2.6 as follows:

$$a_{i} = e^{\rho_{i} * \varepsilon * \ln a_{i} \ln a_{i}}$$

(2.8)

where $\mu_{lnSa}(M,R,T_i$ and $_{lnSa}(T_i)$ are derived from the selected ground motion model, ρ_{i} * is computed using equation and and ε * values are those indicated in Step 1.

As mentioned earlier in this section, once the CMS associated with a period of interest is determined, the ground motion selection algorithm proposed by N. Jayaram et al. (2010) is used to select and modify sets of records that match the target CMS and its variance. The steps of this algorithm are the following:

- Step 1. Parameterize the multivariate normal distribution of lnSa at multiple periods.

  It has been shown that the set of logarithmic spectral accelerations at various periods is a random vector that follows a multivariate normal distribution (N. Jayaram and J. W. Baker, 2008). The parameters of the multivariate normal distribution are the means and variances of lnSa at all periods and the correlations between these values at all pairs of periods. These parameters should be set equal to their target values, which depend on the T* considered.

- Step 2. Perform Monte Carlo simulations to probabilistically generate response spectra from the multivariate normal distribution.

  The number of spectra simulated is equal to the desired number of ground motions to be selected.

- Step 3. For each simulated response spectrum, select a ground motion with a similar response spectrum.

  This similarity is evaluated using the sum of squared errors (SSE):

$$E = \sum_{i=}^{p} \left(\ln a_{\quad i} \right) \ln a_{\qquad i} \right)$$

(2.9)

where $\ln Sa(T_i)$ is the logarithmic spectral acceleration of the ground motion being considered, $\ln Sa^{(S)}(T_i)$ is the lnSa value at period T_i from the simulated response spectrum, and p is the number of periods considered along the range of periods selected.

- Step 4. Apply an optimization technique to further improve the match between the sample and the target means and variances.

  The simulated response spectra have approximately the desired mean and variance, thus the response spectra selected by using this approach will also have approximately the desired mean and variance. However, slight deviations from the target values can happen. The magnitude of these deviations can be estimated by the sum of the squared differences between the target and the sample means and variances (SSE_S) over the period range of interest:

$$E = \sum_{i=}^{p} \left(\hat{m}_{\ln a_{\quad i}} \quad {}^{t}{}_{\ln a_{\quad i}} \quad w \, \hat{s}_{\ln a_{\quad i}} \quad {}^{t}{}_{\ln a_{\quad i}} \right)$$

(2.10)

where $m_{lnSa(Ti)}$ is the mean value of lnSa at period T_i, $\mu^{(t)}{}_{lnSa(Ti)}$ is the target mean value of lnSa at period T_i $_{lnSa(Ti)}$ is the standard deviation of lnSa at period T_i $^{(t)}{}_{lnSa(Ti)}$ is the target standard deviation of lnSa at period T_i, w is the weighting factor indicating the relative importance of the errors in the standard deviation and the mean, and p is the number of periods considered to

compute the error. SSE_S is the parameter to be minimized using the optimization technique proposed herein, which consists in replacing each ground motion selected previously one at a time with a ground motion from the database that results in the best improvement in the match between the target and the sample means and variances, i.e., in the major reduction of the SSE_S value.

Before selecting the ground motions, they are scaled to match the target Sa(T*), or $Sa(T_1)$ in this case. The scaling factors for the unidirectional and bidirectional ground motion studies are exactly the same as those defined in equations 2.1 and 2.2 for the $Sa(T_1)$ scaling method, but in this case, the target $Sa(T_1)$ value comes from the CMS. The following are the expressions of the scaling factors for this method:

- Unidirectional studies. Scale factor for component 1 ($SF_i^{C1}|_{CMS}$):

$$F_i^C{}_C = \frac{a^t}{a_i^C} \tag{2.11}$$

where $Sa(T_1)^{(t)}$ is the target $Sa(T_1)$ derived from the CMS , the subscript CMS refers to the CMS scaling method, and the rest of the parameters has already been indicated previously.

- Unidirectional studies. Scale factor for component 2 ($SF_i^{C2}|_{CMS}$):

$$F_i^C{}_C = \frac{a^t}{a_i^C} \tag{2.12}$$

where all the parameters have already been indicated previously.

- Bidirectional studies. Scale factor for both components ($SF_{i|CMS}$):

$$F_{i|C} = \frac{a_i^t}{\sqrt{a_i^C \, a_i^C}} \tag{2.13}$$

where all the parameters have already been indicated previously.

For the unidirectional studies, four sets of seven scaled records and another set of forty scaled records have been generated, while for bidirectional studies, the group of sets of records generated consists of four sets of seven scaled pairs of records and another set of forty scaled pairs of records.

Figure 2.1 shows the CMS for the first structure, which has a T_1 of 0.9 sec along with the median spectra computed using Campbell and Bozorgnia 2008 attenuation model, and the median spectra plus one and a half times the standard deviation predicted by this model, which gives the target $Sa(T_1)$ to which the CMS is conditioned.

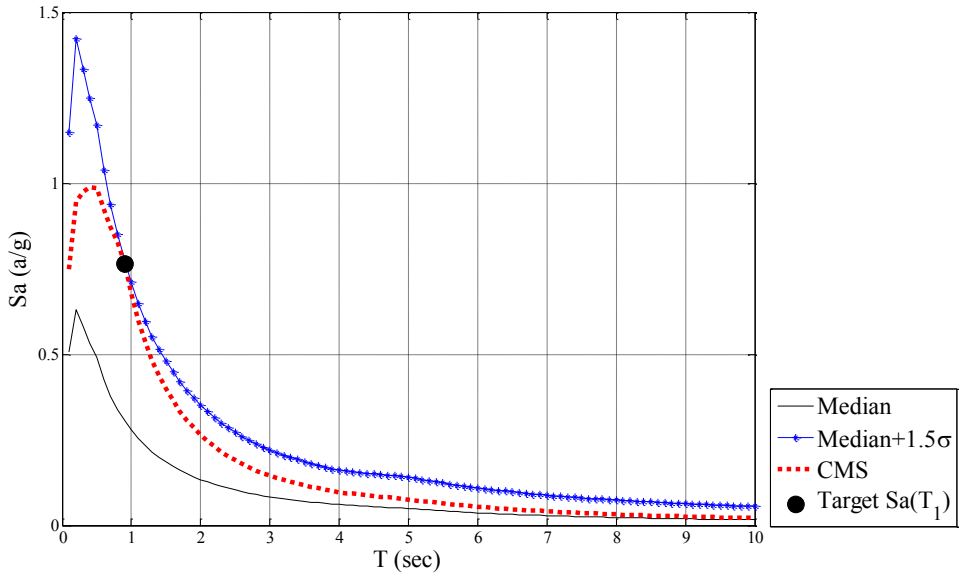

Figure 2.1. C edia n pectr um and e dian pectrum for Bridge A.

It can be clearly seen how the CMS meets the spectrum that is the median plus one and a half times the standard deviation value at T_1 median spectrum Figure 2.2 shows the same CMS but this time with the scaled spectra of those ground motion records belonging to the first set of seven records generated for Bridge A.

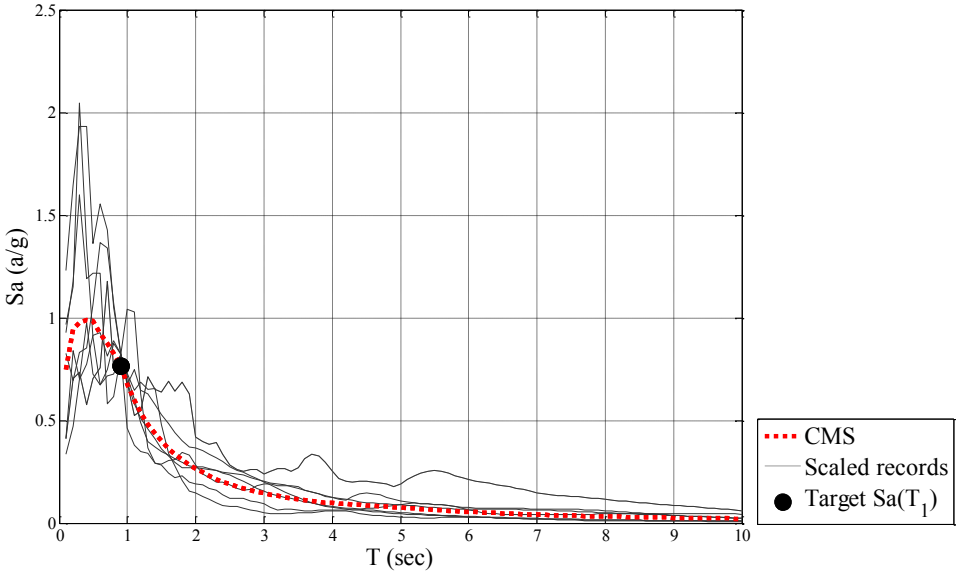

Figure 2.2. CMS and Spectra of Sample Set of Scaled Records for Bridge A.

The figure illustrates how the CMS scaling method scales the ground motions to the target $Sa(T_1)$. The set of records should also match the variability of the CMS. From equation 2.4, the following expression can be derived:

$$\ln a = \varepsilon_{\ln a} \quad \ln a \tag{2.14}$$

Because of ε is the only uncertain parameter in the prediction of the response spectrum, once $Sa(T_1)$ (identified before as $Sa(T^*)$), M and R are given, the standard deviation of $\ln Sa(T)$ conditioned to $\ln Sa(T_1)$ can be written as:

$$\ln a \quad \ln a \quad = \varepsilon \quad \varepsilon \quad \ln a$$

(2.15)

where $_{lnSa(T)|lnSa(T1)}$ is the standard deviation of lnSa(T) conditioned to lnSa(T_1), $\varepsilon \quad \varepsilon$ is the standard deviation of ε conditioned to $\varepsilon_{\ 1}$ and $_{lnSa(T)}$ is the standard deviation of lnSa(T) calculated from the attenuation model used.

Additionally probability calculations lead to equation for $\varepsilon \quad \varepsilon$ (J. W. Baker, 2010):

$$\varepsilon \quad \varepsilon \quad = \sqrt{-\rho \quad *}$$

(2.16)

where all the parameters have already been introduced previously.

From equations and t he next expression for $_{lnSa(T)|lnSa(T1)}$ is derived:

$$\ln a \quad \ln a \quad = \ln a \quad \sqrt{-\rho \quad T_1}$$

(2.17)

where all the parameters have already been introduced before.

From equation 2.17, it is possible to compute the CMS $\pm$ $_{CMS}$ (where $_{CMS}$ = $_{lnSa(T)|lnSa(T1)}$) and plot it along with the CMS and the records spectra to visually check that the variability of the CMS is also matched. Figures 2.3a and 2.3b show this plot. Plotting these spectra in logarithmic scale lets one better appreciate this match.

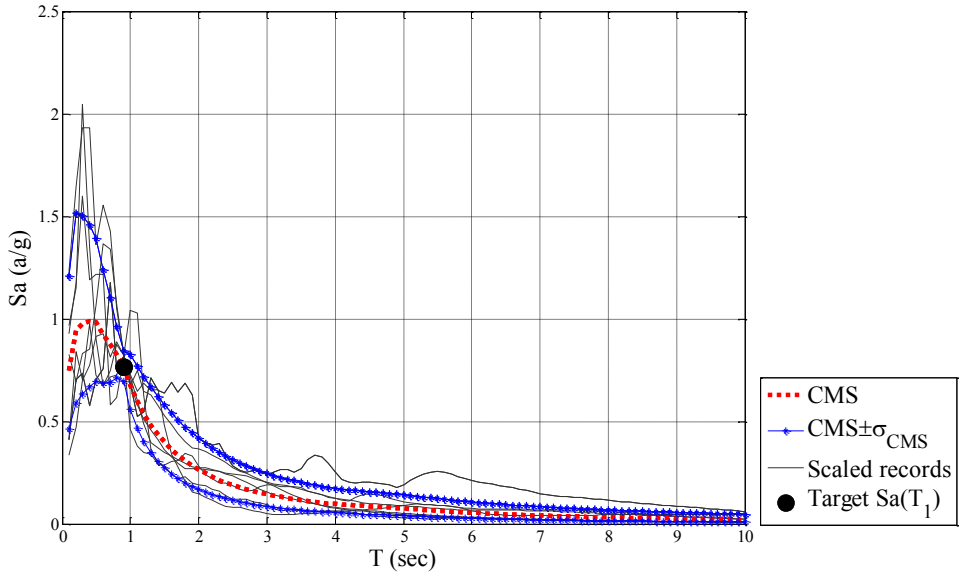

Figure 2.3a. CMS, Spectra of Sample Set of Scaled Records and C ± $_{CMS}$ for Bridge A.

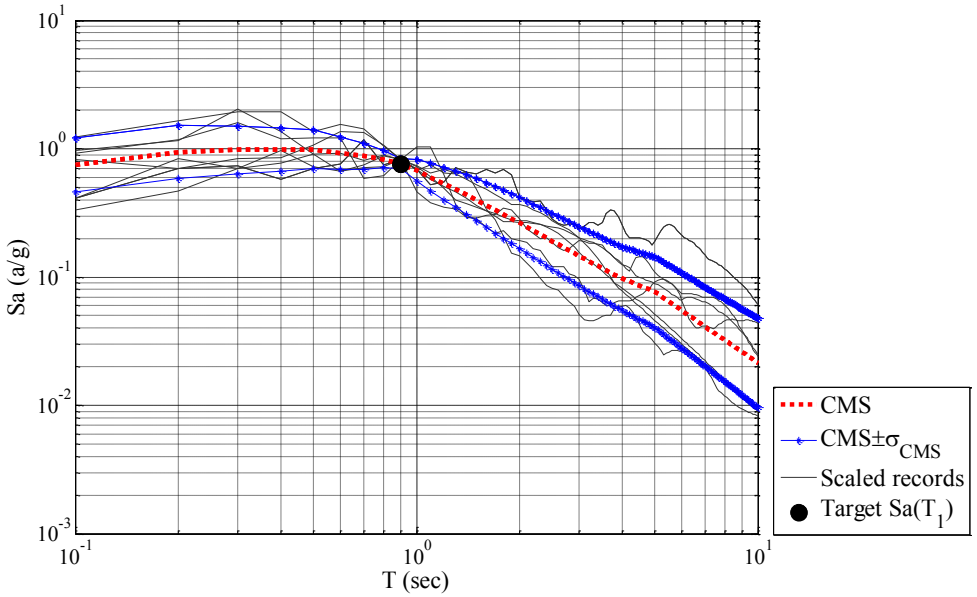

Figure 2.3b. CMS, Spectra of Sample Set of Scaled Records and CMS ± $_{CMS}$ for Bridge A.

CHAPTER 3

TYPICAL BRIDGES USED IN THIS STUDY

3.1. STRUCTURAL DESIGNS, OPENSEES MODELING AND SIDE STUDIES

Six reinforced and prestressed concrete bridges have been selected to conduct the present research project, and they are identified as bridges A, B, C, D, E and F. Bridges A and C are skewed bridges, Bridge B is a straight bridge, and bridges D, E and F are curved bridges. All of them have been designed by the California Department of Transportation, Caltrans, and they have been modeled using the Open Sees (F. McKenna et al., 2000) open-source structural analysis platform.

This section makes a detailed description of the structural designs of these structures and their OpenSees modeling. Additionally, various side studies are also described in detail. The purpose of these side studies is not only to improve the knowledge about the behavior of the bridges considered but also to clarify some modeling issues that have arisen during the modeling process.

3.1.1. Structural Designs

Six reinforced and prestressed bridges designed by Caltrans and located in Los Angeles and Orange counties, are considered in this study. They all meet the criteria for being classified as ordinary standard bridges. These criteria are defined in Section 1.1 of Caltrans Seismic Design Criteria, Version 1.4, 2006, referred to as SDC 2006. If a bridge verifies them, this document can be used as a guide to its design in the state of California.

The selection of the bridges was based on the need to have a manageable number of structures and, at the same time, cover a wide range of bridge geometries commonly used in the Caltrans highway bridge network, in order to be able to generalize the conclusions resulting from the evaluation of the GMSM methods selected. According to these selection criteria, six bridges divided into two groups of three were finally selected. The first group, Group 1, consists of straight and skewed bridges (bridges A, B and C), and the second group, Group 2, consists of curved bridges (bridges D, E and F). Thus all common deck geometries are considered and within a manageable number of structures.

The main characteristics of the selected bridges are described in tables 3.1a and 3.1b. As seen in table 3.1a, Bridge A appears as a skewed type bridge with null skew angle, which is equivalent to refer to it as a straight type bridge. Having changed its type to an equivalent category only seeks to give the table a compact format.

Table 3.1a. Geometry and Properties of Group 1 Bridges

	Bridge A	**Bridge B**	**Bridge C**
Type of bridge	Skewed	Skewed	Skewed
Skew angle	60.0º	0.0º	60.0º
Length	220.6 ft	300.0 ft	418.0 ft
Number of spans	**2** Span 1: 110.3ft Span 2: 110.3ft	**2** Span 1: 150.0 ft Span 2: 150.0 ft	**3** Span 1: 156 ft Span 2: 144 ft Span 3: 118 ft
Type of deck	Prestressed concrete continuous; box girders – multiple	Prestressed concrete continuous; box girders – multiple	Prestressed concrete continuous; box girders – multiple
Deck width	27.1 ft	75.5 ft	77.0 ft
Type of column bents	Single-column	Two-column	Three-column
Columns radius	33.1 in	33.5 in	33.1 in
Columns height	22 ft	22 ft	24.6 ft
Type of abutments	Seat abutments	Seat abutments	Seat abutments

Table 3.2b. Geometry and Properties of Group 2 Bridges

	Bridge D	**Bridge E**	**Bridge F**
Type of bridge	Curved	Curved	Curved
Radius	164.0 ft	551.2 ft	984.3 ft
Length	154.2 ft	501.9 ft	623.4 ft
Number of spans	**2** Span 1: 65.6 ft Span 2: 88.6 ft	**3** Span 1: 150.9 ft Span 2: 200.1 ft Span 3: 150.9 ft	**4** Span 1: 128.0 ft Span 2: 173.9 ft Span 3: 203.4 ft Span 4: 118.1 ft
Type of deck	Reinforced concrete continuous; box girders – multiple	Prestressed concrete continuous; box girders – single	Prestressed concrete continuous; box girders – multiple
Deck width	38.7 ft	35.4 ft	42.0 ft
Type of column bents	Single-column	Single-column	Single-column
Columns radius	33.1 in	53.9 in	41.3 in
Columns height	23.0 ft	35.6 ft	25.8 ft
Type of abutments	Seat abutments	Seat abutments	Seat abutments

3.1.2. OpenSees Modeling

As mentioned at the beginning of the chapter, OpenSees open-source structural analysis platform has been used for modeling the structures. This section describes the properties of the materials selected from the OpenSees materials library to model concrete and steel, specifies the finite elements used to model each bridge component, and defines the damping considered. The mode shapes of the bridges are illustrated at the end.

3.1.2.1. Materials

All structures are reinforced concrete bridges. The concrete considered for modeling the columns is a material available in OpenSees named *Concrete01*, which has no tensile strength, and with a degraded linear unloading-reloading stiffness according to the work of I. D. Karsan and J. O. Jirsa (1969). The core concrete is confined by circular hoops or spirals, while the cover concrete is unconfined. The expected compressive strength for confined concrete is set equal to 6.5 kips, and equal to 5.0 kips for unconfined concrete, according to Caltrans engineers recommendations. The strains associated with these two peak stresses are obtained applying the following expression:

$$\varepsilon_{cy} = \frac{f_{cy}}{E_c} \tag{3.1}$$

where ε_{cy} is the strain associated with f_{cy}, f_{cy} is the expected compressive strength for concrete, and E_c is the tangent modulus of elasticity at the origin of coordinates.

The initial descending curve has the same initial slope for both confined and unconfined concrete since the confining steel has no effect in this range of strains. The expression used to derive the value of E_c is (SDC 2006, Section 3.2):

$$E_c = \quad w \quad \sqrt{f_{ce}} \text{ (psi)} \tag{3.2}$$

where E_c is the modulus of elasticity, w is the unit weight of concrete in lb/ft^3, equal to 143.96 lb/ft^3, and f_{ce}' is the expected compressive strength of the concrete which is equal to the expected compressive strength for unconfined concrete mentioned before.

The E_c value obtained using this formulation is 4030.53 ksi. Once the compressive strength is reached, the unconfined stress falls rapidly to zero at the spalling strength, set equal to 0.005, while the confined stress degrades not as rapidly as the unconfined stress and only till a stress level of 6.0 kips, corresponding to a compressive strain of 0.025. From this point, the stress level remains constant.

These last values are also fixed following the recommendations of Caltrans engineers, who also proposed using *Concrete01* model because its simplicity and the control that one has over the input parameters. However, among the concrete models available in OpenSees, there is an enhanced version of the concrete model proposed by G. A. Chang and J. B. Mander (1994) under the name *Concrete07* (J. Waugh et al., 2008). The authors of *Concrete07* model give the following reasons for having created such material model: (1) the model considers wedging action in the cracks, which makes compression stress develop prior to crack closure; (2) the model behaves differently depending on the moment when the strain reversal occurs, providing a more robust hysteretic behavior; (3) the model proposed by J. B. Mander et al. (1988) is widely used

to determine the confined concrete properties and the model proposed by G. A. Chang and J. B. Mander (1994) extends this last J B and er's model to include the behavior of unconfined and high strength concrete; and (4) G. A. Chang and J. B. Mander used a large number of cyclic concrete tests to validate the model behavior.

Because of these reasons and the rigor of their work developing this enhanced model, its use for this project was considered at the beginning. Although *Concrete01* model was finally selected for this study, it is worthy to see the differences between their backbone curves.

Concrete01 backbone curve is determined based on the values indicated previously. *Concrete07* model requires eight input parameters. Two of them are the expected compressive strength of the concrete and its lateral confining pressure. The first parameter is equal to the aforementioned compressive strength for unconfined concrete, i.e., 5 ksi. The lateral confining pressure is computed according to the properties of the reinforcement of the columns and following the formulation proposed by J. B. Mander et al. (1988):

$$f_{le}=f_l k_e \tag{3.3}$$

where f_{le} is the lateral confining pressure, and:

$$f_l=-\rho_s f_{yh} \tag{3.4}$$

$$\rho_s=\frac{A_{sp}}{d_s s} \tag{3.5}$$

…for circular hoops:

$$k_e = \frac{\left(\frac{ss}{d_s}\right)}{\rho_{cc}} \tag{3.6}$$

…for circular spirals:

$$k_e = \frac{\frac{ss}{d_s}}{\rho_{cc}} \tag{3.7}$$

where A_{sp} is the area of the transverse reinforcement bar, d_s is the diameter of the spiral or hoops between bar centers, s is the center to center spacing or pitch of spiral or circular hoop ss is the clear vertical spacing between spiral or circular hoop bars and ρ_{cc} is the ratio of the area of the longitudinal reinforcement to the area of the core section.

The lateral confining pressure values obtained for the columns of the selected bridges are:

- Bridge A: $f_{le} = 298.3$ psi
- Bridge B: $f_{le} = 277.7$ psi
- Bridge C: $f_{le} = 299.2$ psi
- Bridge D: $f_{le} = 400.3$ psi
- Bridge E: $f_{le} = 534.3$ psi
- Bridge F: $f_{le} = 363.7$ psi

Concrete07 model proposes an expression for E_c. However, in order to better compare the backbone curves, this value has been equated to the E_c value used for *Concrete01* model, which is 4030.53 ksi.

Figures 3.1a and 3.b show the backbone curves of *Concrete01* and *Concrete07* models. It can be seen that for the level of confinement of the columns of bridges A, B and C, the compressive strength of the confined concrete predicted by *Concrete07* model is similar to that of *Concrete01* model, but the corresponding strains differ significantly. For bridges D, E and F, the confinement level is higher, and this is translated into important differences between strains and also compressive strengths values. Another important difference is the post-peak behavior, i.e., the plastic branch of the curves, in all cases. For unconfined concrete, the models do not present significant divergence.

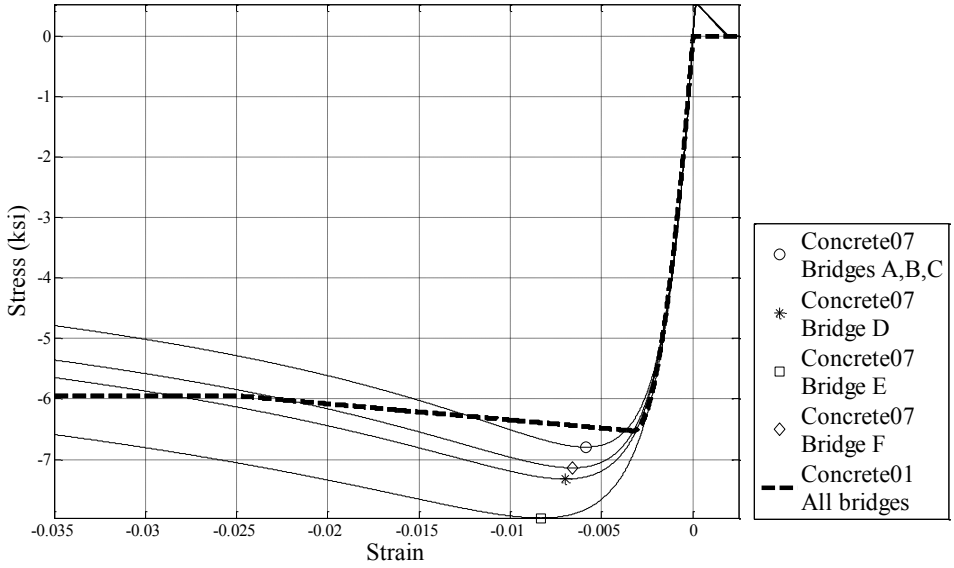

Figure 3.1a. Backbone Curves for Confined Concrete.

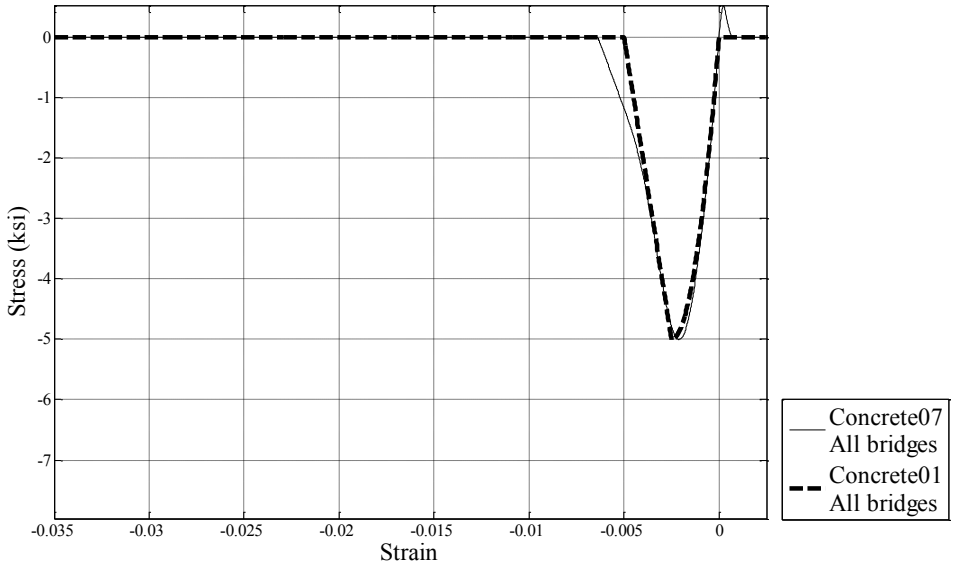

Figure 3.1b. Backbone Curves for Unconfined Concrete.

The differences identified herein suggest conducting a more exhaustive study to quantify potential impact of such differences on the response of the structures.

For modeling the steel of the longitudinal reinforcing bars of the columns, *Steel02* model from the materials library of OpenSees is used, which accounts for isotropic strain hardening after yielding, if desired. The material is assigned an expected yield strength of 68 ksi and a modulus of elasticity of 29000 ksi (SDC 2006, Section 3.2).

3.1.2.2. Deck

To capture the in-plane curvature of curved bridges, the deck should be modeled using a minimum of eight elements per span, or as many elements as necessary so that being the angle swept by one element less or equal to 2º (J. Manterola, 2006). The criterion applied by Caltrans engineers is to use ten elements per span, regardless the geometry of the deck. Taking this into consideration, all bridges are modeled using ten elements per span.

Elastic beam-column elements are used, and, according to SDC 2006, Section 5.6, they are assigned effective moments of inertia I_{eff} and J_{eff}, where I and J denotes moments of inertial for flexure and torsion, respectively, and the subscript eff refers to their effective value. The effective values of the moments of inertia reflect the cracking that occurs before the yield limit state is reached. Bridge D has a conventional heavily reinforced concrete box girder section. Therefore I_{eff} is estimated at $0.75I_g$, where the subscript g refers to the value of the property without considering cracking. No stiffness reduction is recommended for prestressed concrete box girder sections, thus the rest of bridges, because of being all of them prestressed structures with this type of section, are assigned $I_{eff} = I_g$.

A reduction of the torsional moment of inertia is not required for bridges that meet the ordinary standard bridge requirements (SDC 2006, Section 1.1) and do not have a high degree of in-plane curvature. Accordingly, $J_{eff} = J_g$ for bridges A, B, C, E and F, since they are skewed bridges or curved bridges with low degree of in-plane curvature. Although Bridge D has a considerable in-plane curvature, it was decided to assume $J_{eff} = J_g$ for this bridge too, because of its reduced length and its heavily reinforced section.

The Young's modulus used for the elastic beam-column elements is the same as the initial tangent modulus of elasticity defined previously, which is equal to 4030.53 ksi.

All the nodes are assigned translational masses according to their tributary length. Rotational masses are also defined, because they help reproduce more accurately the dynamic response and the fundamental modes associated with the transverse direction. The following expression is used to compute the values of the superstructure rotational masses (A. Aviram et al., 2008):

$$= \frac{d_w}{} = \frac{(m \quad)_{trib} d_w}{}$$

(3.8)

where, M_X is the rotational mass of the superstructure, assigned as lumped mass in axial direction or global X direction, M is the total mass of the superstructure segment tributary to the node, m/L is the mass of the superstructure per unit length, L_{trib} is the tributary length according to the node definition, and d_w is the superstructure width, which is taken as average of bottom and top flanges.

The properties of the nodes are referred to the global coordinate system. For bridges D, E and F, since the deck has in-plane curvature, and assuming that the deck lies on the X-Y plane, the rotational mass of each of its nodes computed according to the above expression is distributed into global X and Y directions as follows:

$$^{node\ i} = \cos\left(\frac{^{element\ i} \qquad ^{element\ i}}{} \right)$$

(3.9)

$$^{node\ i} = \sin\left(\frac{^{element\ i} \qquad ^{element\ i}}{} \right)$$

(3.10)

where, $M_X^{node\ i}$ is the rotational mass of node i associated with global X direction, $M_Y^{node\ i}$ is the rotational mass of node i associated with global direction $^{element\ i+1}$ is the angle between global X direction and element i+1, which is the element that comes after node i and $^{elment\ i}$ is the angle between global X direction and element i, which is the element that comes before node i.

Those degrees of freedom that are not associated with a mass are assigned a mass value equal to 10^{-9} kg, to avoid possible numerical problems during the calculations.

3.1.2.3. Columns

Each column is modeled using five displacement-interpolated beam-column elements with equal length. All the elements are assigned a section defined by the aggregation of the following components:

- A fiber section with core and cover concrete and reinforcing bars. The material model used for concrete is *Concrete01*, as mentioned in the previous section. The corresponding backbone curve is shown in figures 3.1a and 3.1b.
- A material with a linear elastic backbone curve that relates shear force and shear strain. This material provides the element with shear stiffness. The slope of the backbone curve is obtained multiplying the shear modulus, derived from the initial tangent modulus of elasticity, by the reduced area of the column's cross section he reduction factor for circular cross sections is equal to 0.9.
- An elastic material that describes a linear elastic relationship between the torque and the angle of rotation per unit length. This material provides the element with torsional stiffness. The slope of the backbone curve is equal to the multiplication of the shear modulus, the polar moment of inertia of the cross section of the column, and a reduction factor equal to 0.2 (SDC 2006, Section 5.6). Such factor accounts for the great reduction of the torsional stiffness after the onset of cracking.

Therefore the columns have distributed plasticity, which means that they are allowed to go non-linear in all their length. The common practice in bridge engineering is to fix a priori the location and the extension of the plastic hinges, which are those parts of the columns that can reach inelastic behavior. The reasons for considering columns with distributed plasticity in this project are:

- A more realistic structural behavior of the columns is likely to be obtained.
- Although the predicted structural behavior was not more realistic, this study is an opportunity to test the performance of DBE.
- In this study, a procedure to determine the plastic hinge length is developed, and it is based in the ability of DBE to behave non-linear in all their length.

Additionally, at each column there is a sixth element placed on the top that represents the part of the column embedded in the deck. It is a very rigid element and its length is equal to the distance between the bottom slab of the deck and the vertical centroid of the superstructure cross section.

The columns are assigned translational and rotational masses. The expression to compute the rotational masses is the following (A. Aviram et al., 2008):

$$= \frac{}{_{col}} = \frac{(m \quad)_{trib} D_{col}}{}$$

(3.11)

where, M_Z is the rotational mass of the column, assigned as lumped mass in axial direction or global Z direction, M is the total mass of the column segment tributary to the node, R_{col} is half of the average column dimension equivalent to the radius of circular columns, m/L is the mass of the column per unit length, L_{trib} is the tributary length according to the node definition, and Dcol is the column dimension, which can be taken

as the average of the transverses and longitudinal dimensions for cross sections with biaxial symmetry, i.e., the diameter for a circular cross section.

Those degrees of freedom that are not associated a mass are assigned a mass value equal to 10^{-9} kg to avoid possible numerical problems during the calculations.

The modeling of the foundations of the column bents vary depending on the bridge considered. Bridges A, B, C, D and E have pile foundations, while Bridge F has pile shafts. Bridges B and C have multi-column bents, and the foundations of the columns are modeled using pinned connections. Bridges A, D, E and F have single-column bents. For Bridge A, the base of its column is assigned a fixed connection. But for bridges D, E and F, springs are placed at the base of their columns.

The springs were modeled by T. Shantz, Senior Research Engineer from Caltrans Division of Research and Innovation. From column axial load related to both dead and live loads, the percentage of the steel of the columns and their diameter, he generated approximated foundations and their corresponding rotational and translational stiffnesses. Appendix A contains the correspondence with T. Shantz regarding the springs properties.

The rotational and translational stiffnesses of the springs for curved bridges that T. Shantz derived are as follows:

- Bridge D foundations: $K_\theta = 1.8 \cdot 10^8$ kip-in/rad
  $K_H = 300$ kip/in
  $K_{\theta H} = K_{\theta H} \sim 0$ kips
- Bridge E foundations: $K_\theta = 5.0 \cdot 10^8$ kip-in/rad
  $K_H = 830$ kip/in
  $K_{\theta H} = K_{\theta H} \sim 0$ kips
- Bridge F foundations: $K_\theta = 3.6 \cdot 10^7$ kip-in/rad
  $K_H = 1275$ kip/in
  $K_{\theta H} = K_{\theta H} = -179000$ kips

For bridges D and E, since the off-diagonal terms of the stiffness matrix ($K_{\theta H}$ and $K_{H\theta}$) can be considered equal to zero, the springs can be implemented in OpenSees using a zero-length element. However, the off-diagonal terms cannot be considered zero for Bridge F, which implies that there is interaction between rotation and translation. There is not any available element in OpenSees that can take such interaction into consideration. The next paragraph explains how the foundations of Bridge F's columns were modeled to account for the interaction between rotation and translation.

Figure 3.2 shows a two-dimensional bar subjected to bending moments and shear forces with a length o ung's modulus and inertia equal to L, E and I, respectively.

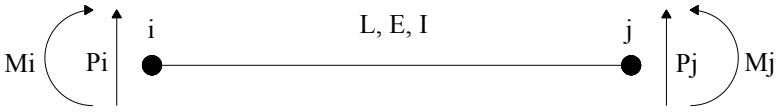

Parameters: Mi: bending moment at *i*; Mj: bending moment at *j*; Pi: shear force at *i*; Pj: shear force at *j*; : length; E: oung's modulus; : inertia

Figure 3.2. Two-Dimensional Bar Subjected to Bending Moments and Shear Forces.

The corresponding stiffness matrix is:

$$= \begin{bmatrix} \underline{E} & \underline{E} & \underline{E} & \underline{E} \\ \underline{E} & \underline{E} & \underline{E} & \underline{E} \\ \underline{E} & \underline{E} & \underline{E} & \underline{E} \\ \underline{E} & \underline{E} & \underline{E} & \underline{E} \end{bmatrix}$$

(3.12)

where K is the stiffness matrix, and the rest of the parameters has already been indicated previously.

Given this stiffness matrix, the governing equation for this problem is:

$$\begin{bmatrix} i \\ i \\ j \\ j \end{bmatrix} = \begin{bmatrix} \underline{E} & \underline{E} & \underline{E} & \underline{E} \\ \underline{E} & \underline{E} & \underline{E} & \underline{E} \\ \underline{E} & \underline{E} & \underline{E} & \underline{E} \\ \underline{E} & \underline{E} & \underline{E} & \underline{E} \end{bmatrix} \begin{bmatrix} v_i \\ \theta_i \\ v_j \\ \theta_j \end{bmatrix}$$

(3.13)

where v_i θ_i, v_j and θ_j are the deflection and rotation at node i and node j, respectively, and the rest of the parameters have already been indicated previously.

Now, consider a cantilever column, i.e., the bar shown in figure 3.2 fixed at node i, thus v_i and θ_i are equal to zero. Therefore the governing equation is:

$$\begin{bmatrix} \\ j \\ \\ j \end{bmatrix} = \begin{bmatrix} \dfrac{E}{} & \dfrac{E}{} \\ \\ \dfrac{E}{} & \dfrac{E}{} \end{bmatrix} \begin{bmatrix} v_j \\ \theta_j \end{bmatrix}$$

(3.14)

where all the parameters have already been indicated in the previous equation.

As mentioned before, the foundations of Bridge F's columns are such that there is interaction between rotation and translation. The rotational and translational stiffnesses of the springs representing the foundations are K_θ and K_H, respectively, and the interaction is represented by $K_{\theta H}$ and $K_{H\theta}$, so the stiffness matrix that governs the response of the columns' foundations is:

$$_F = \begin{bmatrix} H & H\theta \\ H\theta & \theta \end{bmatrix}$$

(3.15)

where K_F is the stiffness matrix of the foundation.

Thus the governing equation is:

$$\begin{bmatrix} F \\ F \end{bmatrix} = \begin{bmatrix} H & H\theta \\ H\theta & \theta \end{bmatrix} \begin{bmatrix} v_F \\ \theta_F \end{bmatrix}$$

(3.16)

where v_F and θ_F are the translation and rotation at the foundations, and P_F and M_F, the shear and the bending moment happening there.

Comparing equations 3.14 and 3.16, one can see that the behavior of the foundations can be modeled by means of a cantilever column such that:

$$\begin{bmatrix} \frac{E}{} & \frac{E}{} \\ \frac{E}{} & \frac{E}{} \end{bmatrix} = \begin{bmatrix} {}_{H} & {}_{H\theta} \\ {}_{\theta H} & {}_{\theta} \end{bmatrix}$$

(3.17)

According to equation 3.17, one obtains another three equations, which are:

$$\frac{E}{} = {}_{H}$$

(3.18a)

$$\frac{E}{} = {}_{\theta}$$

(3.18b)

$$\frac{E}{} = {}_{H\theta} = {}_{\theta H}$$

(3.18c)

For Bridge F, each column has a foundation consisting of a 6.9 ft diameter drilled shaft. A stiffness, i.e., an EI value, of $3 \cdot 10^9$ kip-in^2 was assumed in its modeling (Appendix A). Then, using this stiffness EI, the stiffnesses K_θ, K_H and $K_{\theta H}$ (or $K_{H\theta}$) for Bridge F, and equations 3.18, three values for L are obtained, L_1, L_2 and L_3. The ideal situation would be all these three L values to be exactly the same. However, they are not equal, but they are very close to each other, so it can be assumed that the three equations result in the same L value, which can be taken as the arithmetic mean of L_1, L_2 and L_3. Therefore the foundation of each Bridge F's column can be modeled using a cantilever column with a stiffness EI equal to $3 \cdot 10^9$ kip-in^2 in both horizontal directions of the three-dimensional space, and a length equal to the mean value of L_1, L_2 and L_3.

3.1.2.4. Abutments

The model of the abutments is based on a simplified model developed by A. Aviram et al. (2008) as part of the project they conducted to establish general guidelines for nonlinear analysis of bridges in California. Each abutment is modeled with a rigid element of length equal to the superstructure width connected through a rigid joint to the superstructure centerline, and with a zero-length element at each end with the following characteristics:

- Longitudinal direction. The response is governed by a gap material. The material does not provide stiffness once in tension. In compression, it behaves as an elastic-perfectly plastic material when it reaches the gap length. According to the recommendations of Caltrans engineers, the gap length is derived from the number of spans. It is 1 in for one or two-span bridges, and 1.5 in otherwise. The stiffness and the ultimate strength for an abutment are obtained from SDC 2006, Section 7.8, as follows:

$$_{abut} = \ _{i} w \left(\frac{h}{}\right) \tag{3.19}$$

where K_{abut} is the stiffness of the abutment, K_i is the initial embankment fill stiffness, equal to 20 kip/in/ft based on a large-scale abutment testing at UC Davis, and w and h are the width and the height of the backwall, respectively. The ultimate strength is derived as follows:

$$_{bw} = A_e \quad ksf \left(\frac{h}{}\right) \ ft \ kip \tag{3.20}$$

where P_{bw} is the ultimate strength and A_e is the effective abutment area, obtained by multiplying h and w.

Each abutment has two zero-length elements acting in parallel. Therefore, the stiffness and ultimate strength values assigned to them are half the values obtained for the whole abutment.

- Transverse direction. The response is governed by an elastic material working in both tension and compression. The stiffness and ultimate strength of the whole abutment in transverse direction are obtained as follows: both values are equal to those for longitudinal direction but assuming that the wingwall is 1/3 of the backwall length, and multiplying each quantity by the wall effectiveness coefficient (C_L), equal to 2/3, and also by the participation coefficient (C_w), equal to 4/3. Half the values obtained for the whole abutment are assigned to each zero-length element.
- Vertical direction. The response is governed by an elastic material with zero tensile strength. The stiffness is given by the stiffness of the bearing pads. After reaching a vertical deformation in compression equal to the maximum allowed by these devices, the stiffness changes and tends to infinity.

In transverse direction, the resistance of the brittle shear keys and distributed bearing pads is ignored in this model. The resistance of the shear keys can be computed as follows (A. Bozorgzadeh et al., 2006):

$$= \quad A_{vf} f_y \quad f_c A_c \qquad (3.21)$$

where V_0 is the shear key capacity, A_{vf} is the area of vertical reinforcement crossing shear key-abutment stemwall, f_y is the yield strength of the reinforcing steel f'_c is the concrete compressive strength, and A_c is the area of the shear plane.

Once the shear key capacity is reached, the deck at the abutments is released in transverse direction. Taking this into consideration, the abutments are modeled using the simplified model proposed by A. Aviram et al. (2008), but the ultimate strength of the abutment in transverse direction is taken as the minimum of the value derived using this simplified model and V_0 value.

3.1.2.5. Damping

The damping is evaluated assigning a damping coefficient of 5% to the first two modes of vibration of the structures. The damping matrix is computed using equation 3.22 (M. Paz, 2004, Section 20), which implies damping uncoupling:

[C]=a [ ] a [ ]

(3.22)

where [C] is the damping matrix, [M] is the mass matrix, [K] is the stiffness matrix, and a_0 and a_1 are the coefficients of proportionality, that can be derived from the following equation:

$$_n = -\sum_{i=} a_i \; _n{}^i \quad \text{for n=}$$

(3.23)

where $_n$ and $_n$ are the damping coefficient and the frequency associated to the n^{th} mode of vibration, respectively.

3.1.2.6. Illustrations of the Models

This section shows ground plans of the bridges' models for the reader to have a visual idea of the geometry of such models and also of the geometry of the real structures. It is also used to show the longitudinal direction (X axis) and transverse direction (Y axis) considered in each case. In this study, this issue is especially important for curved bridges, since bidirectional ground motion studies are conducted.

For curved bridges there are no clear criteria to define the longitudinal and transverse directions. A possible and reasonable criterion is to associate the longitudinal axis to the strongest direction, and the transverse axis to the weakest direction. The strongest and weakest directions for all the bridges are determined in the following section. However, this criterion has not been applied herein. The axes for curved bridges shown in figures 3.4a, 3.4b and 3.4c have been set to make the modeling process as agile as possible.

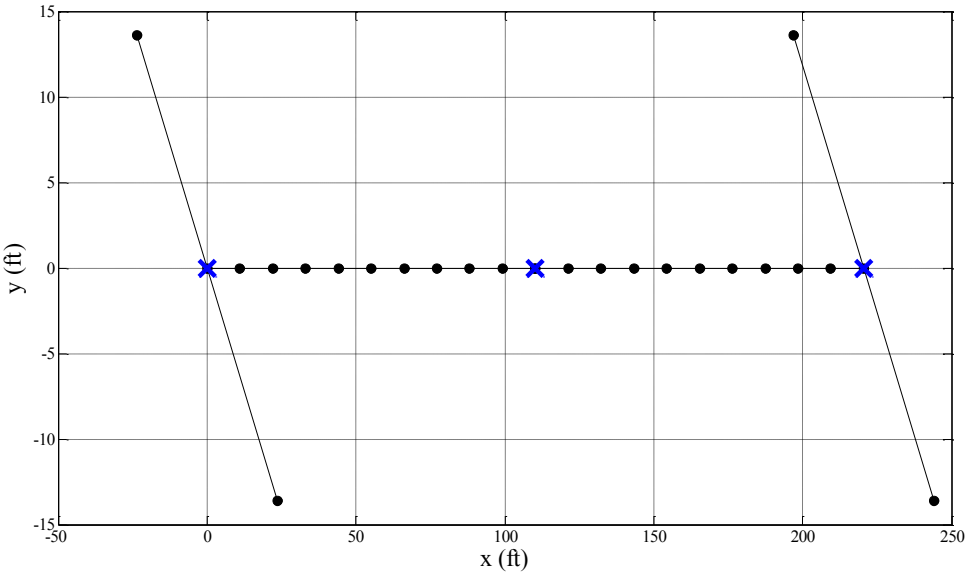

• **Nodes**; **x Nodes indicating the location of abutments and columns**; **- elements**

Figure 3.3a. Illustration Bridge A Model.

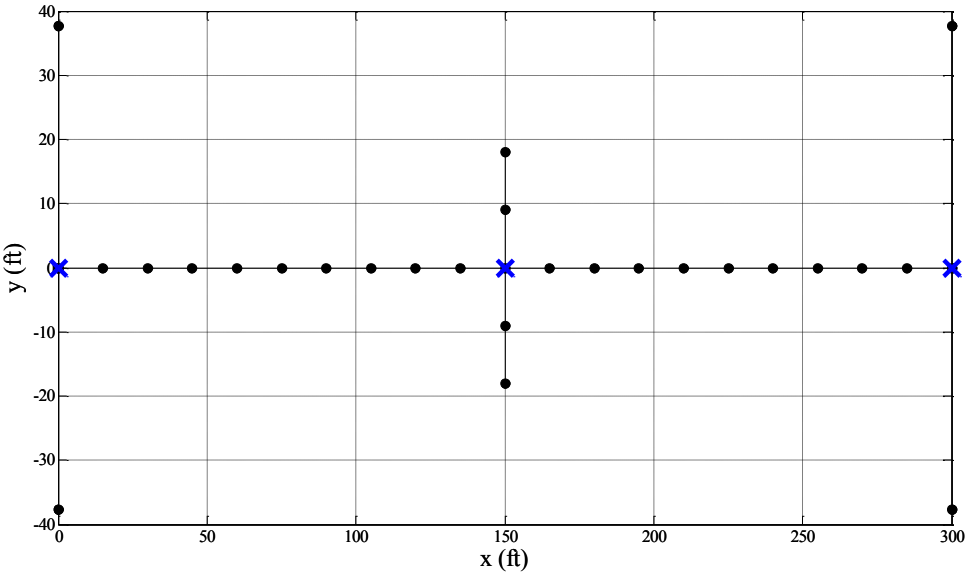

• **Nodes**; **x Nodes indicating the location of abutments and columns**; **- elements**

Figure 3.3b. Illustration Bridge B Model.

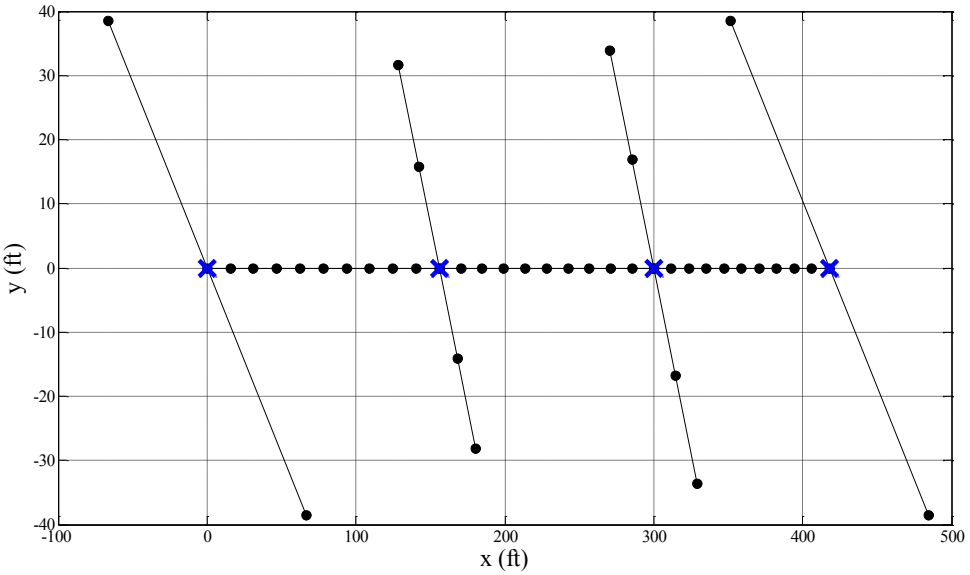

• **Nodes**; **x Nodes indicating the location of abutments and columns**; **- elements**

Figure 3.3c. Illustration Bridge C Model.

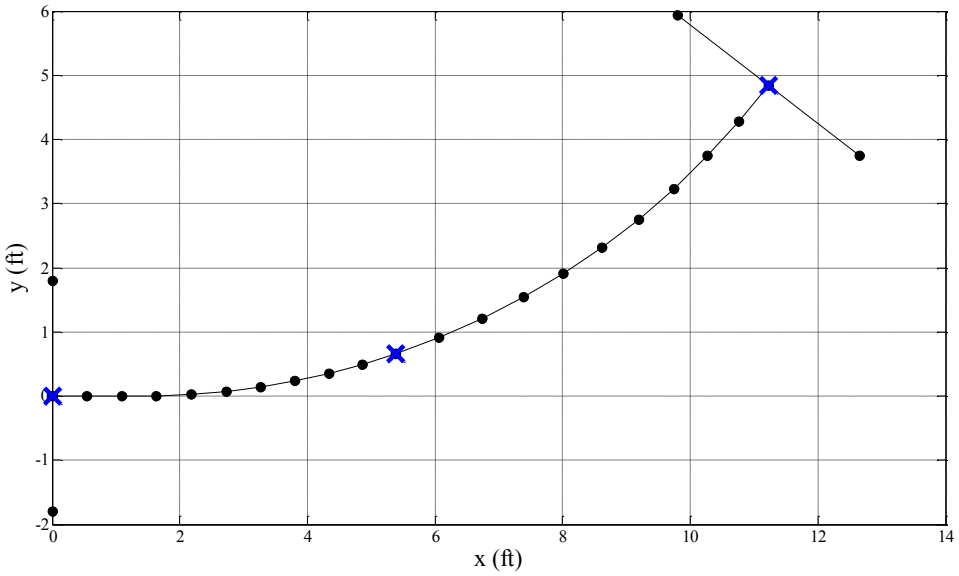

• **Nodes**; **x Nodes indicating the location of abutments and columns**; **- elements**

Figure 3.4a. Illustration Bridge D Model.

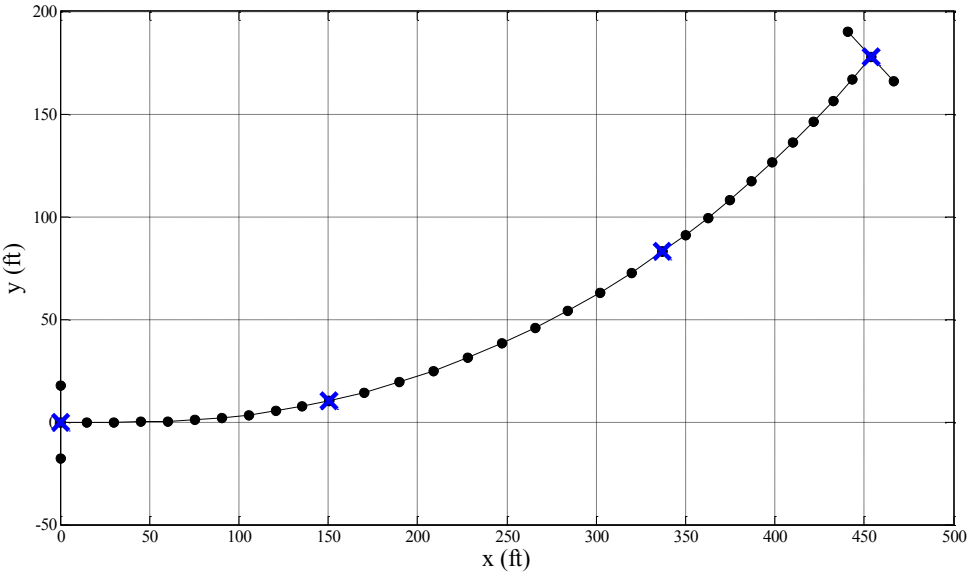

• **Nodes**; **x Nodes indicating the location of abutments and columns**; **- elements**

Figure 3.4b. Illustration Bridge E Model.

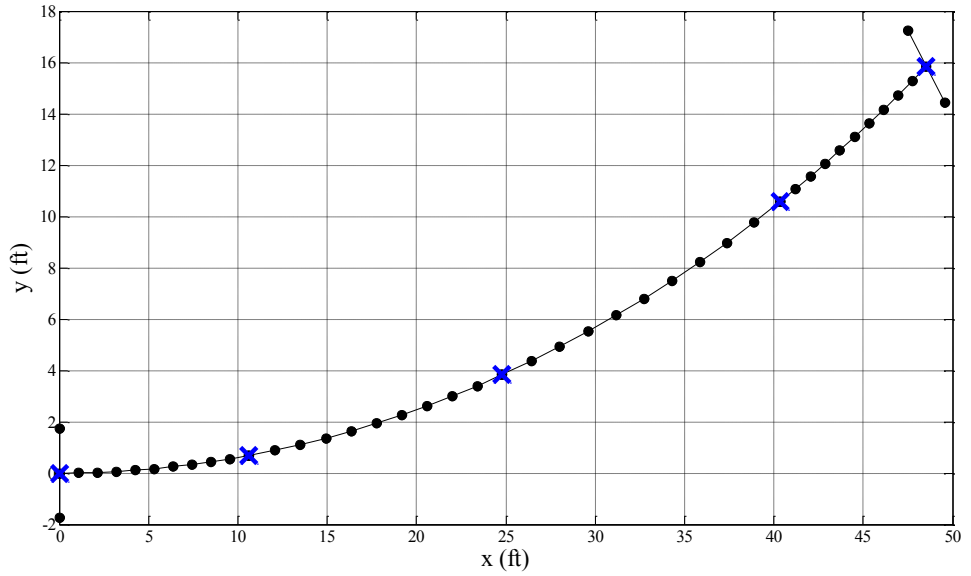

• **Nodes**; **x Nodes indicating the location of abutments and columns**; **- elements**

Figure 3.4c. Illustration Bridge F Model.

3.1.3. Side Studies

During the modeling process of the structures, various challenging issues arose. The next side studies have been conducted to resolve such challenging issues.

3.1.3.1. Displacement-Based and Force-Based Elements

The columns of all six bridges are modeled considering distributed plasticity. As mentioned before, they are modeled using five displacement-interpolated beam-column elements with a cross section being defined by a fiber section. This fiber section consists of a series of fibers which are assigned elastic-plastic materials. The fibers corresponding to concrete are assigned a material model with the backbone curve shown in figures 3.1a and 3.1b, while those corresponding to steel are assigned an elastic-plastic material with isotropic strain hardening after the yielding stress. As discussed when presenting these two materials, an important step is the material model selection.

This section discusses the selection of a proper type of finite element model for modeling bridge columns in this project. The aim is to determine available element models in OpenSees, i.e., displacement-interpolated (DBE) or force-interpolated (FBE) beam-column elements, that present better numerical stability and, at the same time, give more accurate results. Several studies have been conducted addressing this issue from different points of view, and there is extensive literature presenting the fundamentals of these two types of elements and proposing numerical solutions to solve the respective disadvantages. Efforts are also being done to gather the advantages of both elements into a single element (e.g., B. N. Alemdar and D. W. White, 2005). So the aim of the present section is to determine the most appropriate element to use for this project.

The experience acquired in this project shows that DBE presents less convergence problems. For curved bridges, given a particular structure and a ground motion to be applied to it, the simulation could perfectly succeed using DBE but fail using FBE. Five elements per column and five integration points per element were used in all cases. The following pushover analysis was conducted to determine the viability of using DBE with this number of elements per column and integration points per element.

The geometry and materials of the column used to pursue the pushover analysis are those of Bridge D's column. This column has a length of 23 ft and a circular cross section with a diameter of 5.5 ft. Any axial force is applied during the pushover analysis, and the column is pushed 0.55 ft, which corresponds to a drift ratio of 10%.

The following combinations of number of elements and number of points of integration are tested:

- Group 1: 2 elements per column considering 2, 5, 8 and 10 integration points per element.
- Group 2: 5 elements per column considering 2, 5, 8 and 10 integration points per element.
- Group 3: 10 elements per column considering 2, 5, 8 and 10 integration points per element.

Each group of combinations is tested with both types of elements. Table 3.2 shows the results obtained. The errors shown in this table are referred to the solution obtained using 10 integration points per element. By solution it is meant the value of the base shear related to a certain value of the displacement of the top of the column.

Table 3.2. Pushover Analysis

Integration points	Minimum error		
	2 elements	**5 elements**	**10 elements**
DBE-2	$0.030 \cdot 10^{0}$	$0.004 \cdot 10^{0}$	$0.001 \cdot 10^{0}$
DBE-5	$5.490 \cdot 10^{-4}$	$1.704 \cdot 10^{-4}$	$8.662 \cdot 10^{-5}$
DBE-8	$2.869 \cdot 10^{-4}$	$6.471 \cdot 10^{-5}$	$1.958 \cdot 10^{-5}$
FBE-2	$0.264 \cdot 10^{0}$	$0.083 \cdot 10^{0}$	$0.032 \cdot 10^{0}$
FBE-5	$0.177 \cdot 10^{0}$	$0.045 \cdot 10^{0}$	$0.015 \cdot 10^{0}$
FBE-8	$0.185 \cdot 10^{0}$	$0.045 \cdot 10^{0}$	$0.015 \cdot 10^{0}$
(DBE-5 – FBE-5)/FBE-5	$0.175 \cdot 10^{0}$	$0.045 \cdot 10^{0}$	$0.015 \cdot 10^{0}$

The results show that considering more than 5 elements is unnecessary for DBE, since the reduction of the error is not significant. For FBE, this is not as clear as for DBE. What is definitely clear for both elements is that considering more than 5 integration points per element is unworthy. Therefore 5 is the optimum number of integration points. For 5 integration points per element, and assuming that FBE give the exact solution, taking more than 5 DBE per column can be considered unnecessary, since the order of magnitude of the errors is less than 5%, thus it is concluded that the optimal combination for DBE is 5 elements per column and 5 integration points per element.

The height of the columns is approximately the same for all bridges, except for Bridge E's columns, which are 35.6 ft height. So for bridges A, B, C and F, the optimal combination derived from the pushover analysis is considered to be valid, assuming that different column diameters does not affect the results significantly.

The same pushover analysis is conducted for the same column but changing its height to 35.6 ft. Similar results to those exposed in table 3.2 are obtained in this case, thus the optimal combination for this height is also 5 elements per column and 5 integration points per element.

Figure 3.5 shows the results of the pushover analysis for both DBE and FBE, considering 5points of integration and variable number of elements per column. As seen in this figure, the pushover curves do not decay. This fact will be addressed later, when presenting a method to determine the plastic hinge length.

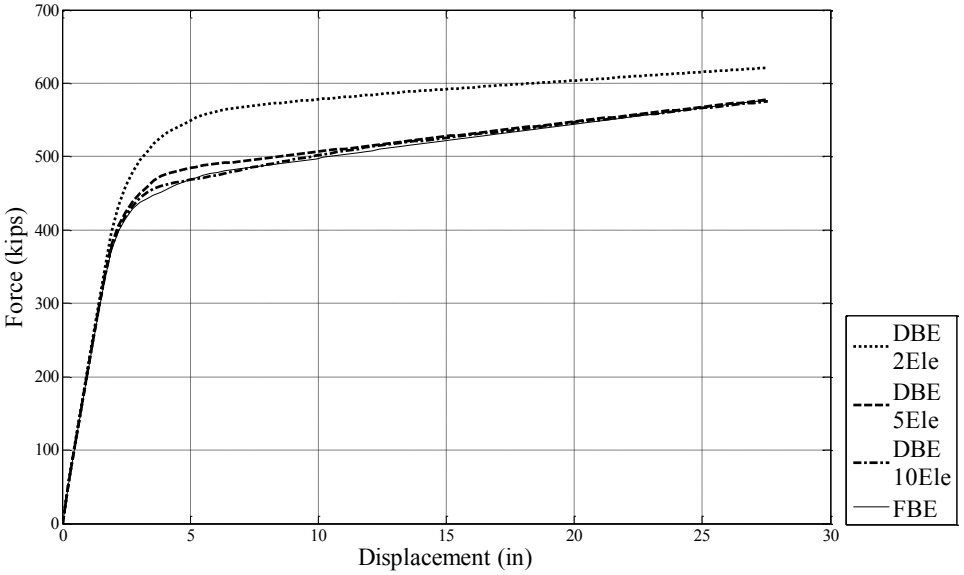

Figure 3.5. Pushover Curves for DBE and FBE.

3.1.3.2. Pushover Analysis of the Bridges

As discussed previously, a possible criterion to establish the longitudinal and transverse direction of a bridge is to associate these directions to those of maximum and minimum strength of the structure, respectively. The strength of a bridge can be understood as the peak force value of its pushover curve, or the force level at the maximum displacement allowed in the analysis in those cases in which the curve does not decay.

In this section, each bridge is subjected to a pushover analysis every 5º in order to determine the strongest and weakest directions. A total of seventy-two pushover analysis per bridge are conducted. They consist in pushing the bridge under study in its center of

masses, and stop the pushover analysis when the drift ratio of the shortest column reaches a value of 10%. The displacement of the center of masses and the sum of the reactions at the supports in the direction of the push define the pushover curve.

The following figures contain the results. For each structure, they show the maximum force level reached in each pushover analysis normalized by the maximum of the seventy-two maximums recorded. 0º angle is associated with positive X axis and positive rotation is counterclockwise.

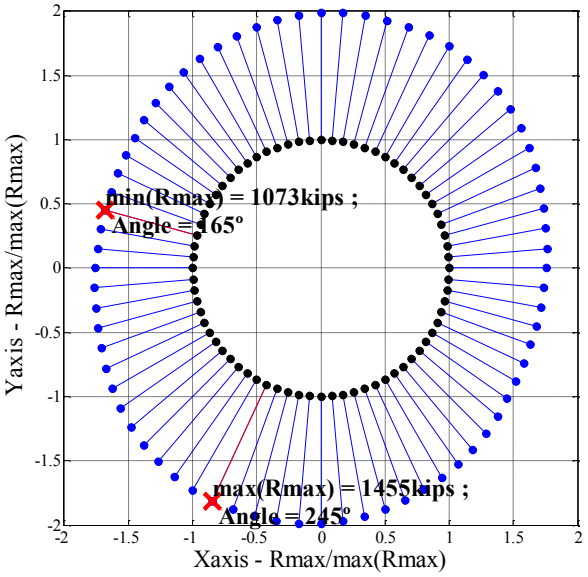

Figure 3.6a. Pushovers Bridge A.

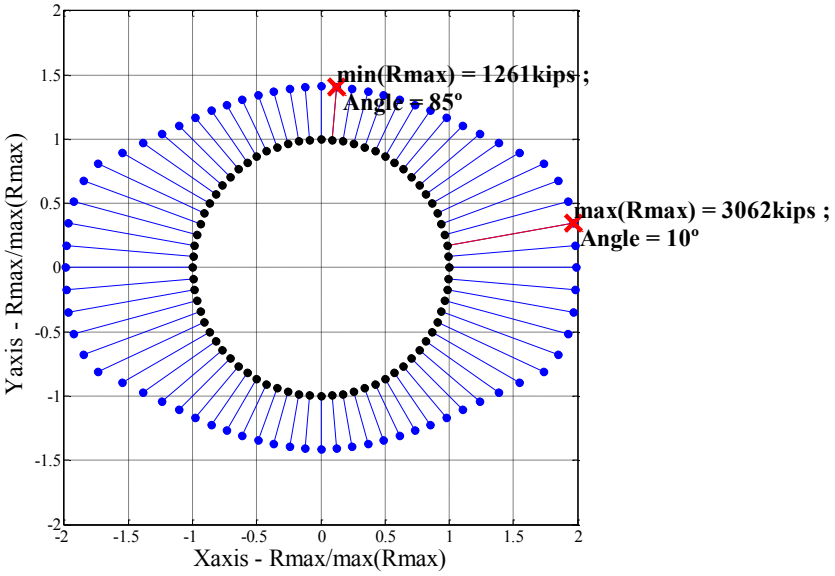

Figure 3.6b. Pushovers Bridge B.

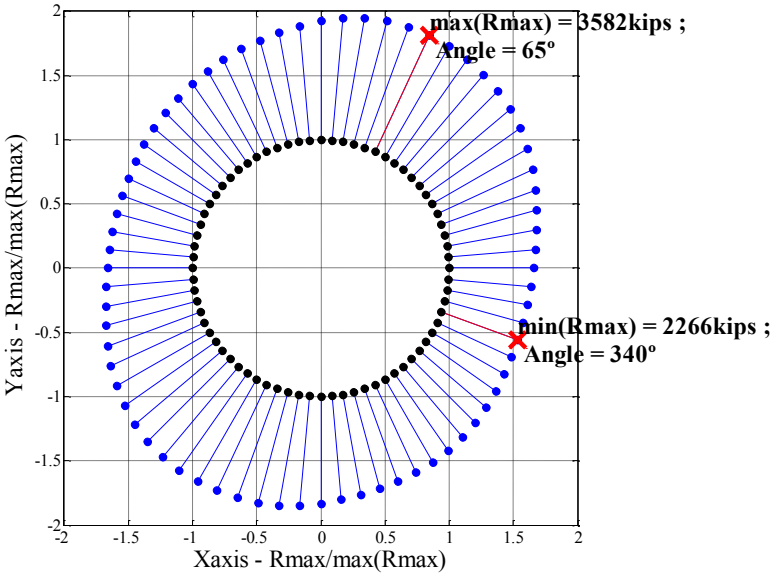

Figure 3.6c. Pushovers Bridge C.

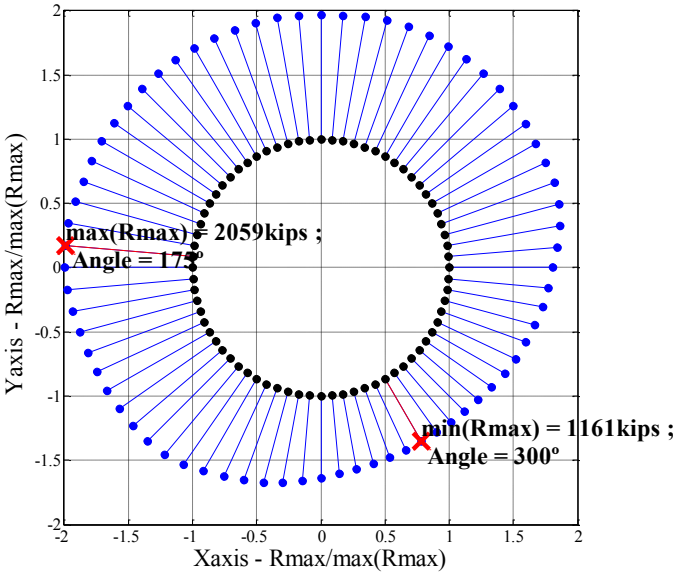

Figure 3.7a. Pushovers Bridge D.

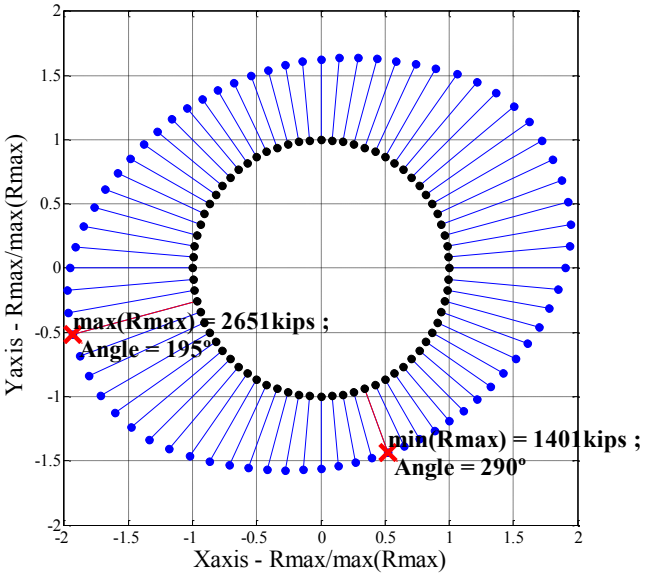

Figure 3.7b. Pushovers Bridge E.

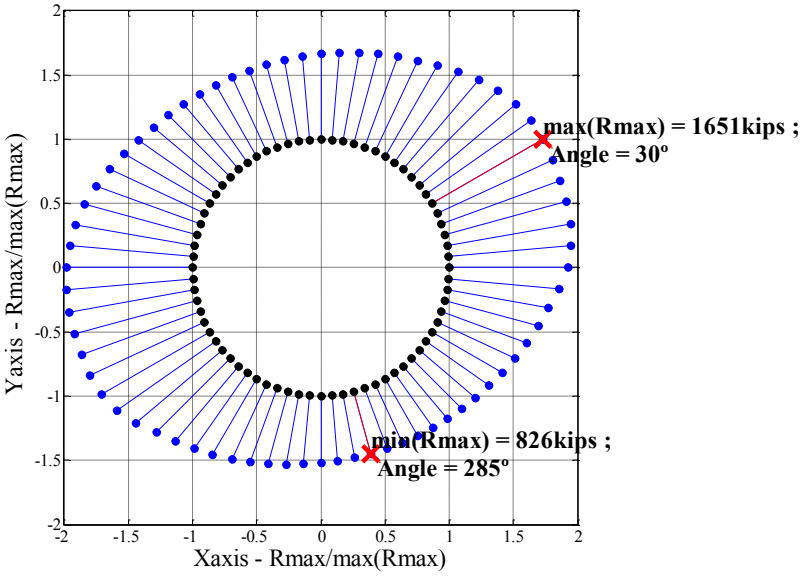

Figure 3.7c. Pushovers Bridge F.

The results for Bridge B show that the longitudinal or X axis defines the strong direction, while the transverse or Y axis, the weak direction, according to the aforementioned criterion to define such axes. Unlike Bridge B, bridges A and C have almost opposite distribution of strengths, due to their skew. Their strongest direction is not perpendicular to the abutments, as expected a priori. The reason might be an overestimation of the transverse capacity associated to the shear keys.

For curved bridges, none of which is perfectly symmetric, the results are reasonable. Bridges E and F are the ones with a highest degree of symmetry with respect to an axis perpendicular to the bowstring defined by the edges of the abutments and passing through its middle point. The strongest direction for them is approximately parallel to this bowstring, and the weakest is perpendicular to it. Bridge D meets this criterion for the weakest direction, but not for the strongest. However, it does not mean that the response is unreasonable or unexpected: first of all, the strongest direction is perpendicular to one of the abutments, which makes sense, and secondly, this is the bridge with less degree of symmetry, and one cannot expect a distribution of strengths as uniform and symmetric as the distribution of strengths associated with bridges D and F.

The fundamental periods of the bridges are computed from this side study. Such periods should be associated to the effective properties of the structures. The properties of the deck are already considered in their effective values, according to Section 3.1.2.2. However, for the columns, since they are modeled using nonlinear beam-column elements with their cross section represented by a fiber section, it is not possible to explicitly consider the effective value of their properties. In order to account for the

cracking of the columns in the determination of the fundamental period, the following solution has been applied.

For each pushover analysis, the fundamental period of the bridge is computed when the bottom section of all columns is at least 50% cracked. To determine the percentage of cracking of a section, the next procedure is followed:

- At each step of the pushover analysis, determine the tensile strains of each longitudinal bar in the section.
- Compute the tensile strain associated with concrete cracking in tension, which is the strain related to a stress equal to 10% of the compressive strength of unconfined concrete.
- Determine the number of bars exceeding the strain associated with concrete cracking in tension. The percentage of cracking of the section is obtained by dividing this number by the total number of longitudinal bars in the section, and then multiplying this result by one hundred.

The fundamental period of the bridge is then taken as the arithmetic mean of all the fundamental periods computed, one per each pushover analysis, i.e., a total of seventy-two fundamental periods. The values obtained are:

- T_1 Bridge A: 0.87 sec
- T_1 Bridge B: 1.27 sec
- T_1 Bridge C: 1.63 sec
- T_1 Bridge D: 1.23 sec
- T_1 Bridge E: 0.94 sec
- T_1 Bridge F: 1.93 sec

The value of the fundamental periods of the structures has been shown to be very sensitive to various modeling factors, e.g., the effective properties of the deck. The springs at the base of the columns of curved bridges D, E and F have incremented the periods with respect to those obtained considering fixed connections. The in-plain curvature of the deck of these bridges is another factor, but not related to modeling, that influences the value of their fundamental period. Given exactly the same bridges but with their decks being straightened, the fundamental periods are lower.

3.1.3.3. OpenSees Ground Motion Treatment

When performing dynamic analysis there are two time steps to consider: the time step of the dynamic analysis itself, and the time step of the record being applied to the structure. The number of steps in which to compute the analysis is also an input. This side study intends to clarify how OpenSees performs when these two time steps do not coincide, and when the time step of the analysis multiplied by the number of steps of the same results in a value that is larger than the duration of the record.

The first step is to create a model from which being able to record the accelerations that are applied to the structure given an input ground motion. This model consists of a two-dimensional elastic beam-column element infinitely rigid, with unit length, with unit mass at the top, and fixed in all its degrees of freedom at the bottom. Recording the base shear of this model should be equivalent to recording the accelerations being input. Next figures show the input ground motion used for this side study and the base shear recorded. It can be seen that the base shear values at each time

step are equal to the input accelerations, thus this model can definitely be used as a tool to record the accelerations that OpenSees applies to a model given an input ground motion.

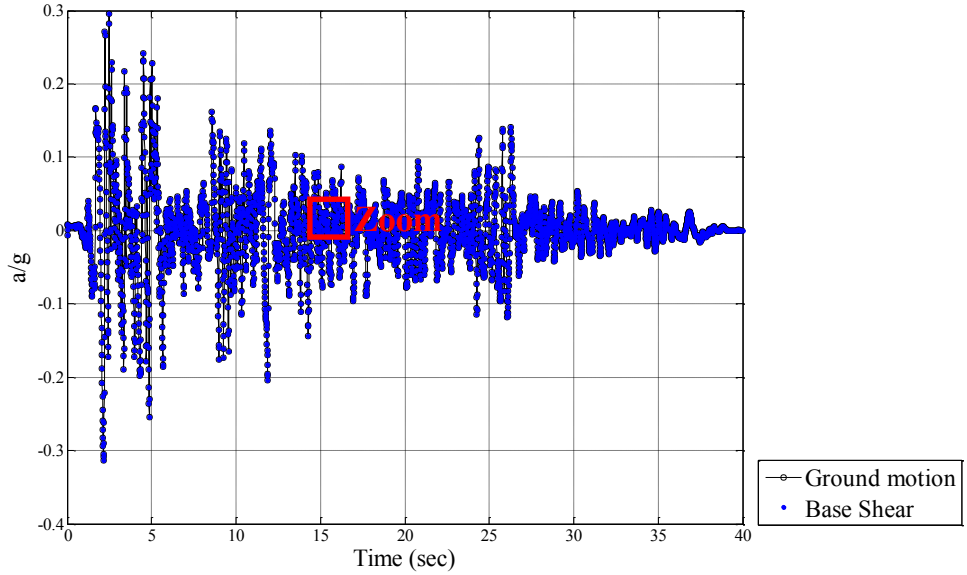

Figure 3.8a. Ground Motion Accelerations and Base Shear.

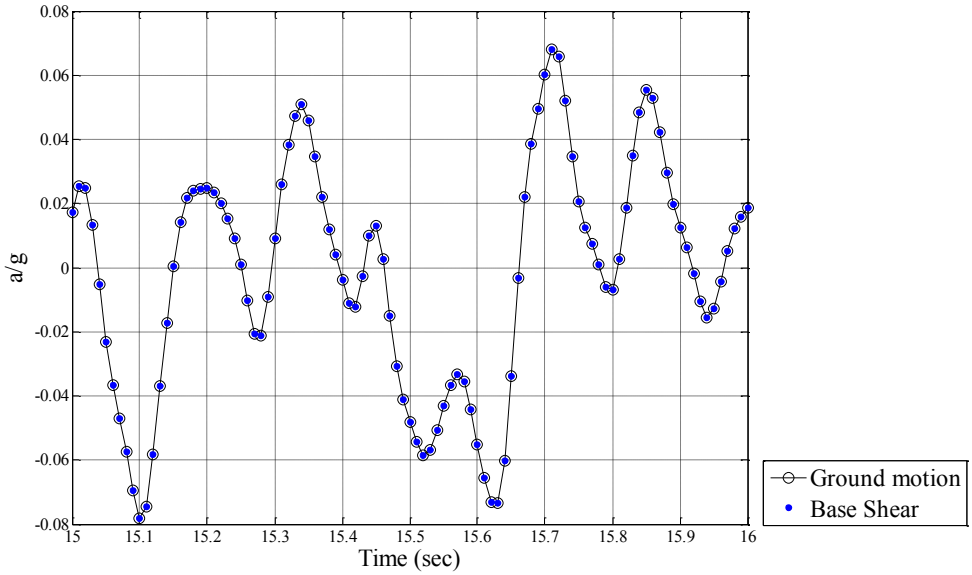

Figure 3.8b. Zoom Indicated in Figure 3.8a.

The following are the different cases considered for the purpose of this side study and the corresponding conclusions:

- Case 1. Analysis time step equal to ground motion time step, and number of steps equal to twice the number of points of the ground motion record.

  Figures 3.9a and 3.9b show the results for this case. It can be seen that when the time of the analysis is larger than the time of the record, OpenSees considers null accelerations.

- Case 2. Analysis time step equal to half the ground motion time step, and number of steps equal to the number of points of the ground motion record.

  Figures 3.10a and 3.10b illustrate the results for this second case. They show that when the time step of the analysis is shorter than the time step of the record, OpenSees does linear interpolation to determine the acceleration values when necessary.

- Case 3. Analysis time step equal to one and a half times the ground motion time step, and number of steps equal to the number of points of the ground motion record.

  This last case is presented in figures 3.11a and 3.11b, which show that when the time step of the analysis is larger than the time step of the record, OpenSees also does linear interpolation to determine the acceleration values when necessary. After the maximum time of the record, OpenSees considers null accelerations.

- Figures Case 1:

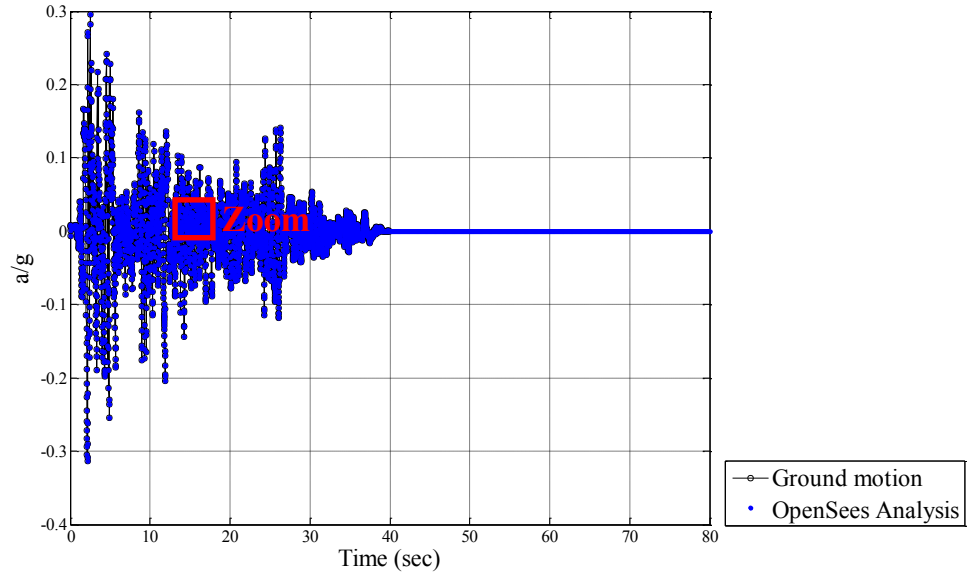

Figure 3.9a. Ground Motion and OpenSees Analysis Accelerations (Case 1).

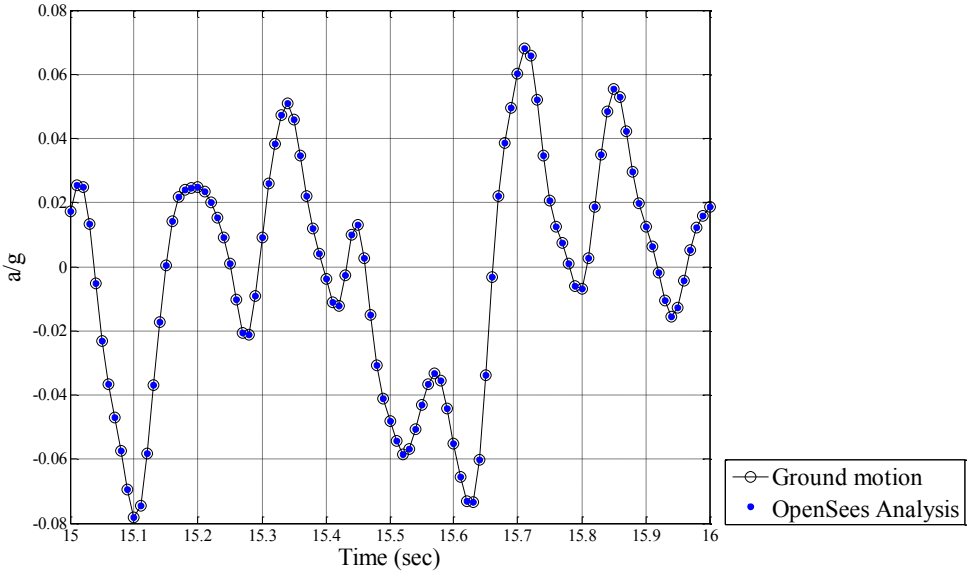

Figure 3.9b. Zoom Indicated in Figure 3.9a.

- Figures Case 2:

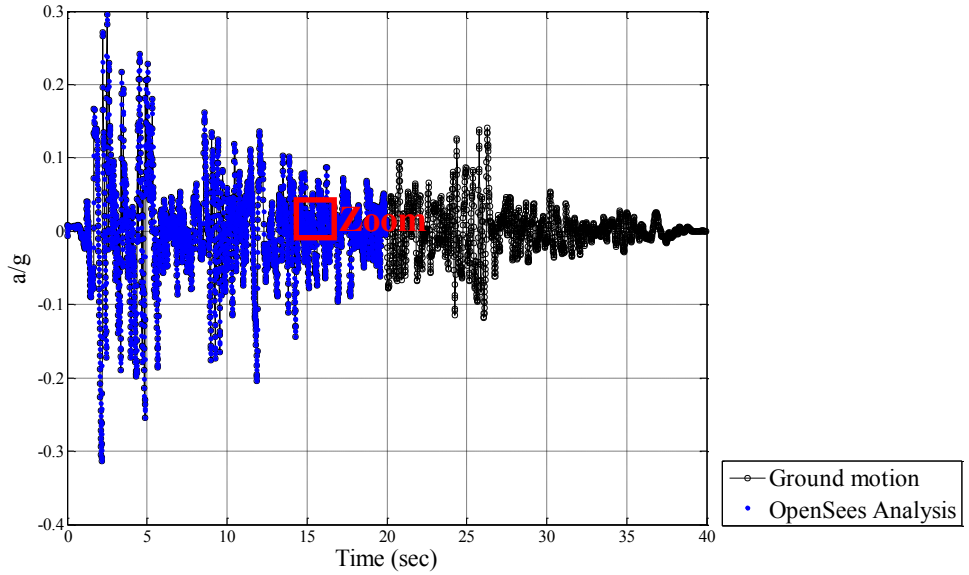

Figure 3.10a. Ground Motion and OpenSees Analysis Accelerations (Case 2).

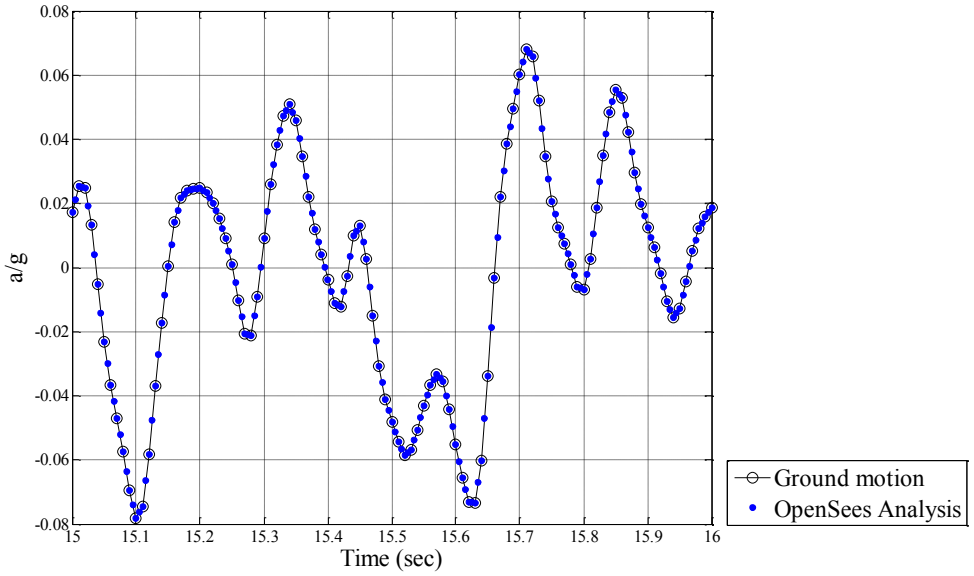

Figure 3.10b. Zoom Indicated in Figure 3.10a.

- Figures Case 3:

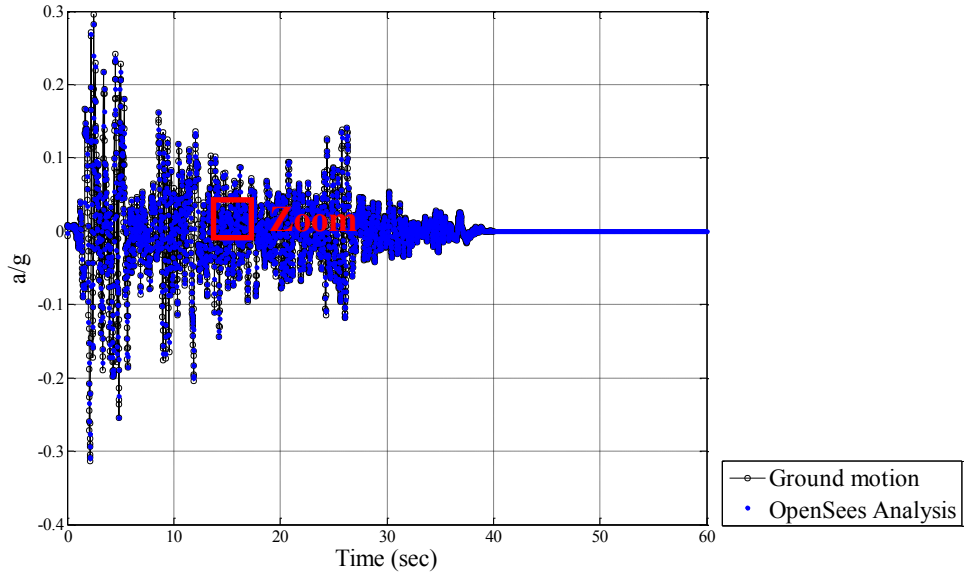

Figure 3.11a. Ground Motion and OpenSees Analysis Accelerations (Case 3).

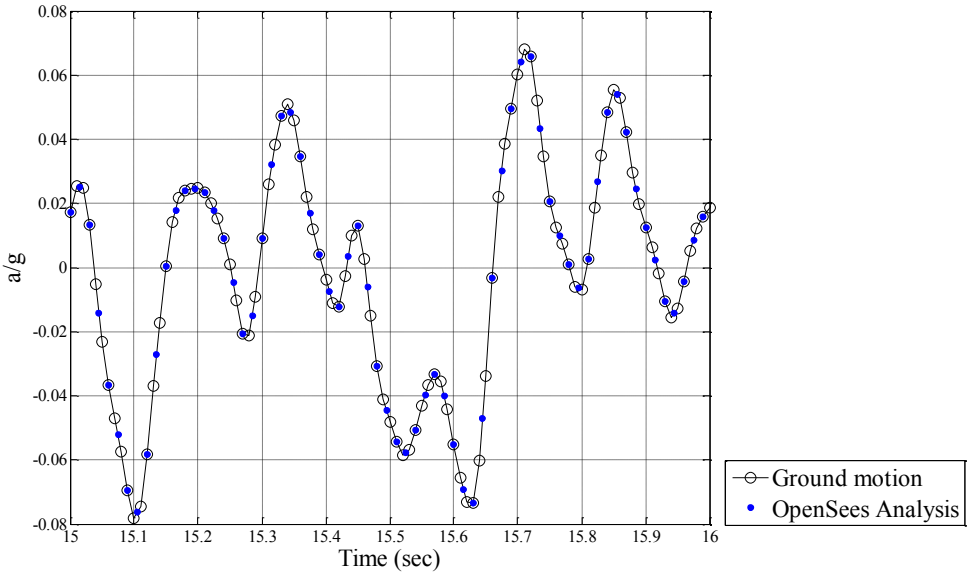

Figure 3.11b. Zoom Indicated in Figure 3.11a.

3.1.3.4. Method to Determine the Plastic Hinge Length

A procedure to determine the plastic hinge length of the columns is proposed in this last side study. As mentioned when explaining the modeling of the columns, this procedure is based on the ability of the finite elements to behave non-linear in all their length, i.e., finite elements with distributed plasticity. This method is being improved, and the efforts are focused on enhancing its accuracy and on making it applicable to those cases where it needs to be applied many times.

To explain this procedure, a model consisting of a cantilever column with a mass at the top has been created. The column is the same as the Bridge D's column, and the mass is equal to half of the mass of the deck of this bridge. The column is modeled using five displacement-interpolated beam-column elements with five integration points per element. Element 1 is the bottom element, and Element 5 is the one on the top. The rest of the elements are numbered accordingly. The integration points of each element are numbered similarly: given an element, Section 1 refers to the lower integration point, and Section 5 refers to the upper integration point. For the displacement-interpolated beam-column elements used herein, the integration along the element is based on the Gauss-Legendre quadrature rule, so mapping each element from -1 to 1, the distribution of the integration points along its length is as follows:

- Coordinate Section 1: $- (1/21)\cdot(245+14\cdot (70)^{1/2})^{1/2}$
- Coordinate Section 2: $- (1/21) \cdot (245-14\cdot (70)^{1/2})^{1/2}$
- Coordinate Section 3: 0
- Coordinate Section 4: $+ (1/21) \cdot (245-14\cdot (70)^{1/2})^{1/2}$
- Coordinate Section 5: $+ (1/21) \cdot (245+14\cdot (70)^{1/2})^{1/2}$

The same ground motion used for the previous side study but amplified by a factor of 8 is applied to the column to assure intense nonlinear behavior.

The method proposed herein follows the next steps:

- Step 1. At each time step, record the bending moment and the axial force at each integration point.
- Step 2. For each axial force, compute the corresponding plastic moment capacity of the cross section according to SDC 2006, Section 3.3. Therefore, at each time step, three values are related to each integration point, i.e., bending moment, axial force and the corresponding plastic moment capacity.
- Step 3. Identify those integration points where the bending moment is equal to its corresponding plastic moment capacity. The integration points where this happens can be considered part of the plastic hinge.

The history of the bending moments and the corresponding plastic moment capacities for the first two elements of the column are shown in figures 3.12a and 3.12b. Only the first five seconds are shown for Element 1, and only the range from ten to fifteen seconds for Element 2, because it is at these periods of time when the bending moment equates the corresponding plastic moment capacity at some integration points for the first time. All the integration points of Element 1 reach their plastic moment capacity. The same happens to Element 2, except for its last integration point, which does not reach the plastic moment capacity. These points are highlighted in the figures. Only the first two elements of the column are shown because the rest do not reach the plastic moment capacity at any integration point. In the legend of the figure, PM stands for plastic moment capacity, and BM stands for bending moment.

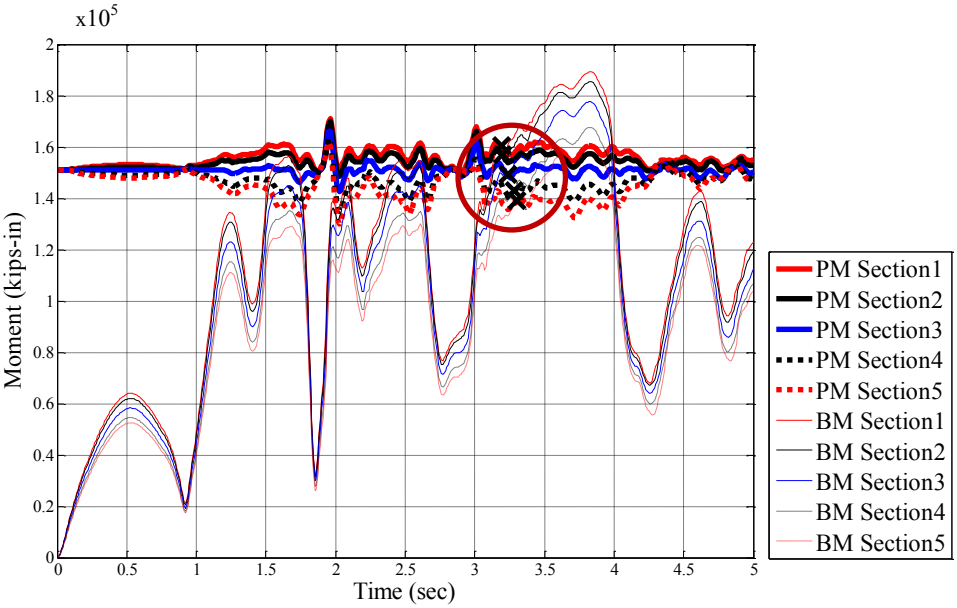

Figure 3.12a. History of Bending and Plastic Moments (Element 1).

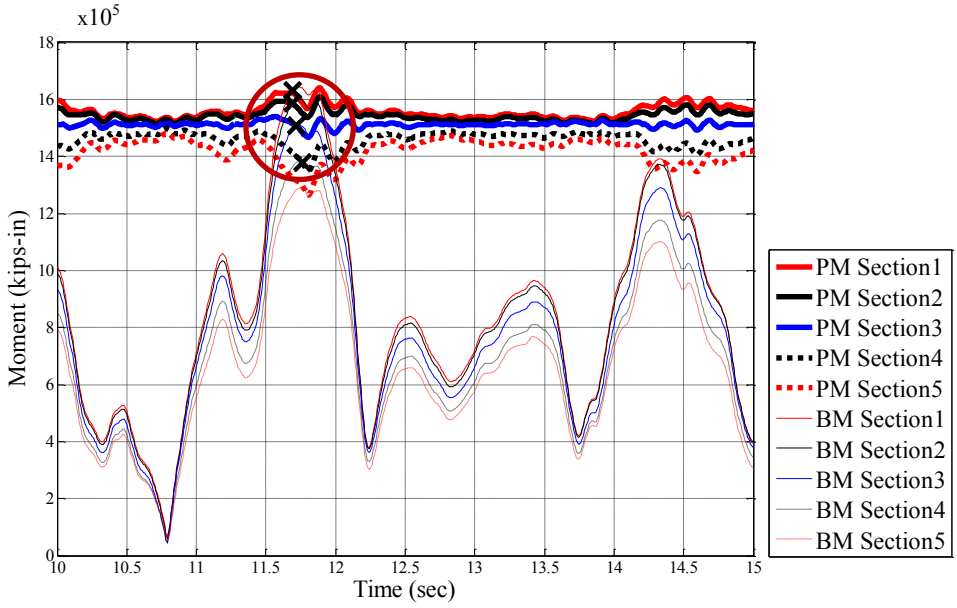

Figure 3.12b. History of Bending and Plastic Moments (Element 2).

From these results, figure 3.13 can be plotted. It shows the moment when the integration points reach the plastic moment capacity for the first time. It provides a visual idea of the evolution of the plastic hinge length during the earthquake.

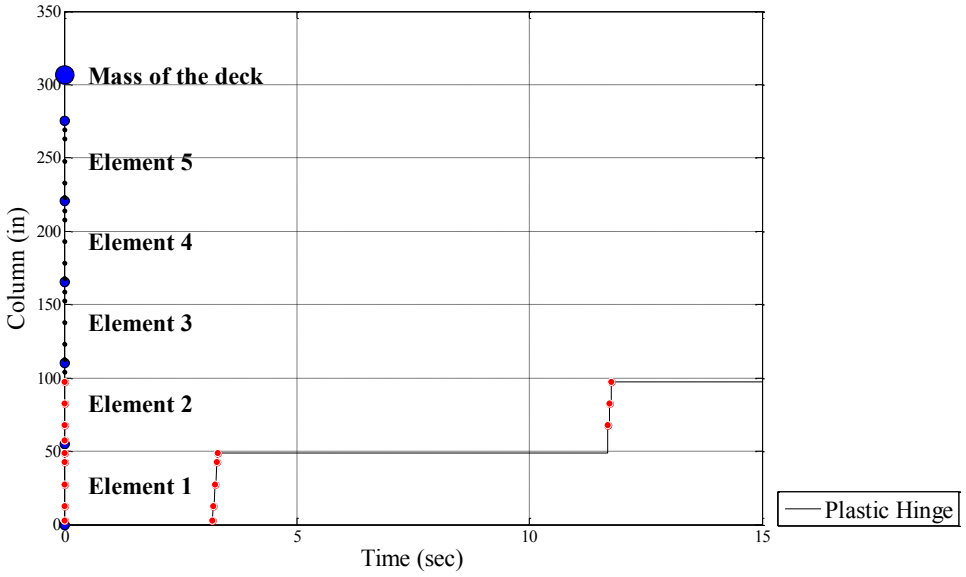

Figure 3.13. Plastic Hinge Length.

There is an important inconsistency in these results, which is the fact that the bending moments exceed the plastic moment capacities, as it can be seen in figures 3.12a and 3.12b. There are two reasons that explain this conflicting situation. They are (1) the way of determining the plastic moment and (2) the material models used.

According to SDC 2006, Section 3.3, the plastic moment capacity of the cross section is calculated by a moment-curvature analysis based on the expected material properties. The moment-curvature curve is idealized with an elastic perfectly plastic response. The elastic portion of the idealized curve passes through the point that marks the moment when the first reinforcing bar yields. The idealized plastic moment capacity is obtained by balancing the areas between the actual and the idealized moment-curvature curves beyond the first reinforcing bar yield point. Figure 3.14 illustrates this procedure.

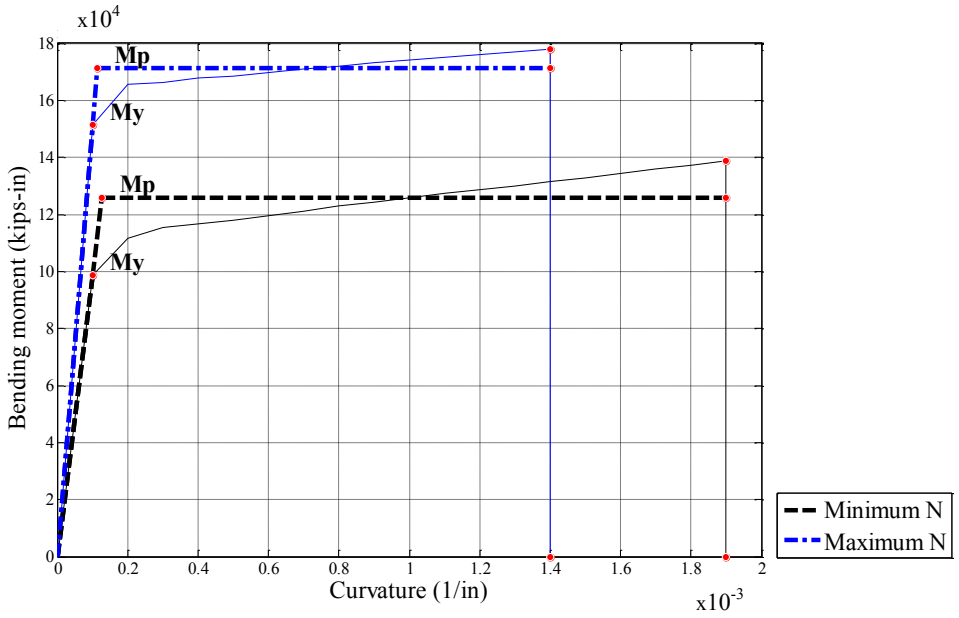

Figure 3.14. Moment-Curvature Curves and Corresponding Idealizations.

The two moment-curvature curves correspond to the maximum and the minimum axial forces in compression reached in Section 1 of Element 1. In the legend of the figure, N stands for compressive axial force, My stands for the moment for which the first rebar yields, and Mp stands for the plastic moment capacity.

Therefore the plastic moment capacity is underestimated. This underestimation aggravates if the ultimate curvature of the cross section is not determined accurately. For this example, the ultimate curvature of the cross section is determined as the curvature for which at least one of the reinforcing bars reaches a strain in tension equal to 0.09, or at least one point of the core concrete exceeds a strain in compression of 0.025. The former value is determined according to SDC 2006, Section 3.2, while the latter is based on experience. However, the best way to determine the ultimate curvature would be recording the curvature that happens right before the failure of the cross section. This is not possible herein because of the material models used: (1) the steel model consists in an

elastic-plastic material with isotropic strain hardening after yielding, and it never dies; (2) the concrete model, although it degrades after yielding in compression, the backbone curve becomes flat after a certain level of strain and stress, as seen in figure 3.1a. A cross section with these two material models will never fail because its materials never die.

To verify that these are the reasons that make the results be inconsistent, the isotropic strain hardening of the steel after yielding is suppressed, so the backbone curve after this pick stress becomes flat. With this new material model for the steel, moment-curvature curves similar to the one shown in figure 3.15.

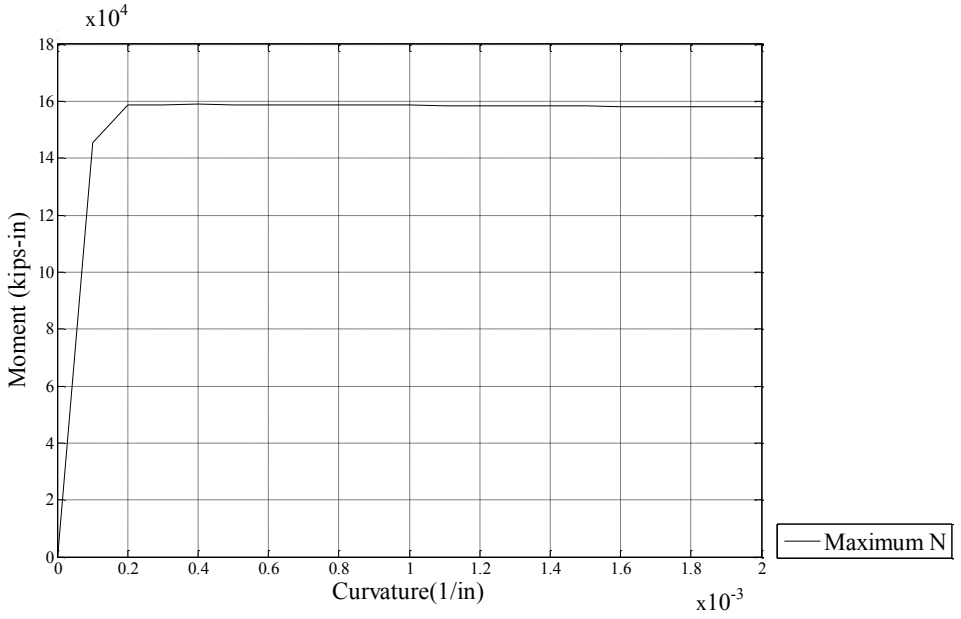

Figure 3.15. Moment-Curvature Curve.

For these shape of the moment-curvature curve, the plastic moment capacity of the cross section is equal to the moment associated to the flat branch. There is no need to do the idealization shown in figure 3.14.

Therefore using this modified material model for steel, which results in moment-curvature curves that allow to determine the plastic moment capacity of the cross section

accurately, consistent results are expected. Figures 3.16a and 3.16b show the results for Element 1 obtained using such modified material model for steel and applying a ground motion scaled by a factor of 5 instead of 8.

The figures illustrate what was expected a priori: before the collapse of the structure, the cross sections of the first element reach but not exceed their plastic moment capacity. Although not shown herein, the same happens to Element 2. These results proof the validity of the procedure but evidence the need to account for accurate and realistic material models.

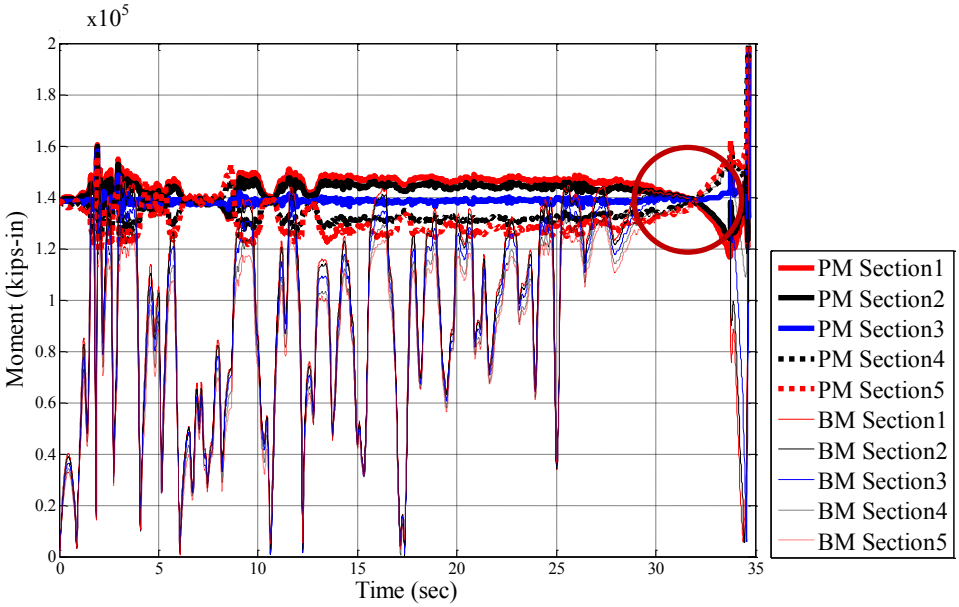

Figure 3.16a. History of Bending and Plastic Moments (Element 1).

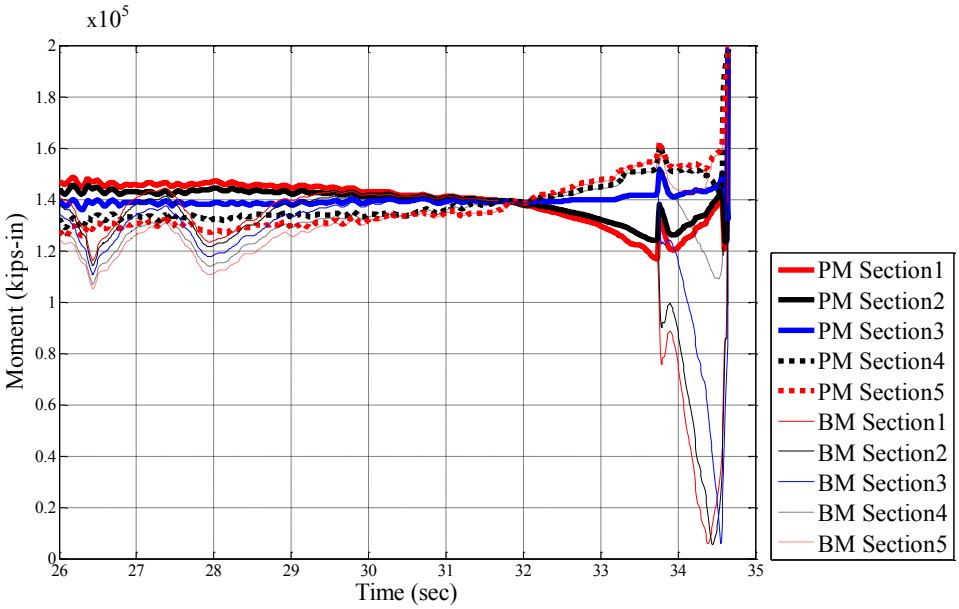

Figure 3.16b. Area Highlighted in Figure 3.16a.

3.2. OBJECTIVE OF NONLINEAR DYNAMIC ANALYSIS

The goal of nonlinear dynamic analysis is the prediction of the bridges' response. This response can be described by different engineering demand parameters (EDPs). Those selected in this study are the maximum displacement of the top of the columns and the maximum displacement of the deck at the abutments. Both EDPs control the structural capacity of the bridges, the first in terms of the columns' strength and the second in terms of deck unseating.

CHAPTER 4

EVALUATION OF GMSM METHODS IN ESTIMATING BRIDGE ENGINEERING DEMAND PARAMETERS (EDPs)

4.1. GROUND MOTION SCENARIO

The starting point of any GMSM method is to define a target ground motion scenario. In this study, the ground motion scenario is the following: an M 7.0 earthquake occurring on a strike-slip fault, at a site that is 10 km from the fault rupture on soil with a shear wave velocity for the top 30 m of its profile ($V_{S,30}$) equal to 400 m/s. The ground motion for this scenario must have a spectral acceleration demand at the first mode of the structure (Sa(T_1 that is one and a half standard deviations above the median predicted value determined using the Campbell and Bozorgnia 2008 attenuation model. This last constraint can be referred to as being the ground motion a " ε motion". The spectrum associated with this ground motion scenario is shown in figure 2.1b, Chapter 2.

This target ground motion scenario is selected because of being consistent with the so common 2% in 50 years motions and maximum credible earthquake (MCE) ground motions used in the current building code provisions for high seismic sites in California. This ε motion scenario is chosen because % in years and CE ground motions have Sa values that are larger than the median Sa associated with the controlling scenario event therefore referred to as ε motions C B Haselton et al. (ATC, 2008), using the full set of United States Geological Survey (USGS) deaggregation data Harmsen et al showed that the average value for ε is for a % in years motion at high seismic California sites, being the maximum equal to 2. Moreover, there

are some regions where the MCE ground motions are characterized by having an $Sa(T_1)$ value of one standard deviation above the median spectral acceleration predicted for the ground motion scenario considered A ε value of is a compromise solution that balances all this ε values commented

4.2. POINT OF COMPARISON

Once the target ground motion scenario is defined, the GMSM methods can be applied to generate different sets of ground motions, selected and modified according to the procedure that characterizes each method.

The next step is to apply these sets of ground motions to the bridges and compare and contrast their structural responses. As mentioned in Chapter 3, the structural response of each bridge is determined by the following two EDPs: the maximum displacement of the top of the columns and the maximum displacement of the deck at the abutments. As pointed in the same Chapter 3, the former EDP controls the structural strength of the structure, while the latter, the possibility that the deck unseats during the earthquake. All those cases that result in the collapse of the bridge being tested are excluded from the sample, being a sample a particular set of ground motions. Collapse happens when the structural capacity of the columns is exceeded, or there is unseating of the deck, or both. The structural capacity of the columns is defined by a certain maximum value of its drift ratio, while unseating happens when the maximum displacement of the deck at the abutments exceeds the length of the seat.

Excluding the collapsed cases makes computing the statistical measures of bridge responses unreliable. Due to this lack of reliability, only the median of the EDPs is

considered. Therefore all GMSM methods selected target Objective 4, explained in Chapter 2, and the evaluation of such methods consists in comparing and contrasting the median value of the EDPs chosen.

In the reference research project referred to in Chapter 2, the bridge responses obtained applying de two selected GMSM methods are also compared to the POC or high-end prediction As mentioned in Chapter OC stands for "point of comparison" and it is an estimation of the true response of the structures. The POC is not computed herein. However, an explanation of how to compute this prediction of the true bridges' response is exposed next.

The POC should be computed following the same strategy applied by GMSM Working Group (C. B. Haselton et al., 2009), but using an expanded version of the M 7.0 set of ground motions this group used, since bidirectional ground motion studies are also conducted in the present study. The criteria to select the ground motions would be the following:

1. < <
2. km < km
3. m s
4. Lowest usable frequency of 0.25 Hz

The first three criteria are set to achieve an accurate approximation of the target ground motion scenario. As already commented in Chapter 2, R is the source-to-site distance, and the restraint on $V_{S,30}$ implies considering soil classes from A to D. The ground motions finally selected would be applied to the structures.

Although the POC is not computed, these four criteria are used to select a bin of one hundred and seventeen pairs of ground motion records representative of the target ground motion scenario. The two GMSM methods evaluated in this research work select ground motion records from this bin.

Because of bidirectional ground motion studies being conducted in this project, not one but two POCs would be created, one for unidirectional motions (1D-POC) and another for bidirectional motions (2D-POC).

The approach used to obtain the two POCs would be the same as the approach considered by J. Watson-Lamprey (C. B. Haselton et al., 2009), which is divided into the following four steps:

1. Perform structural analysis using the ground motions selected to compute the POC and record the two EDPs of interest from each analysis, along with the relevant properties of each ground motion.
2. By using regression analysis, develop a predictive equation that relates ground motion properties and the structural responses obtained.
3. By using ground motion prediction equations, predict the distribution of ground motion properties that will occur during the target earthquake scenario.
4. Evaluate the regression equation over the predicted distribution of ground motion properties, to compute the distribution of structural response. The resulting distribution of the structural response is the POC.

4.3. EVALUATION OF THE GMSM METHODS SELECTED

As indicated in Chapter 2, the following are the groups of ground motions generated by $Sa(T_1)$ scaling and CMS scaling methods and applied to the bridges:

- $Sa(T_1)$ scaling method sets:
    - Set 1 (bidirectional)

      It consists of 42 pairs of records selected and scaled according to the principles of this method. The scaling factors depend on the value of the fundamental period of the structures, but the un-scaled pairs of records are the same for all of them. The components of each pair are applied simultaneously, the first in longitudinal direction and the second in transverse direction.
    - Set 2 (unidirectional)

      It consists of 84 records, which are the two components of the previous 42 pairs, considered individually and scaled differently. Again, the scaling factors vary depending on the fundamental period of the structures. These 84 records are applied only in longitudinal direction.
- CMS scaling method sets:
    - Set 1 (bidirectional)
        - Subset 1

          The first set has 7 pairs of records selected and scaled according to the principles of this second method. Like Set 1 of $Sa(T_1)$ scaling Method, these pairs are applied to the structures in both longitudinal and transverse directions simultaneously. However, in this case, not only the scaling factors but also the un-scaled records vary from bridge to bridge.

- Subsets 2, 3 and 4

  These sets are similar to set 1 but with other scaling factors and selected records.

- Subset 5

  40 pairs of records define this fifth set. Each pair is properly scaled and applied to the bridges in longitudinal and transverse directions simultaneously. Similar to sets 1, 2, 3 and 4, the scaling factors and the un-scaled records also vary from bridge to bridge.

- Set 2 (unidirectional)

  It is similar to the first set of this method, but instead of pairs, individual records are considered in this case.

Next tables show the median of the EDPs selected to describe the structural responses of the bridges. Bridge F is not analyzed here in. The first EDP shown (EDP1) is the maximum displacement in the unseating direction of the zero-length elements that simulate the abutments divided by the gap size, which is equal to 11 in for all bridges. The second EDP (EDP2) is the maximum drift ratio of the bents. Collapse happens when EDP1 > 1 or EDP2 > 8%.

The numbering of the bents is such that Bent 1 is the first bent starting from the left abutment of the bridges. The orientation of the structures is shown in figures 3.3a, 3.3b and 3.3c for skewed bridges, and in figures 3.4a, 3.4b, 3.4c for curved bridges.

BRIDGE A

Table 3.3.1a. Bridge A. Max Abut Disp/Gap Size. Bidirectional Studies

	ZL-1 TOP	ZL-1 BOTTOM	ZL-2 TOP	ZL-2 BOTTOM
Set Sa(T_1)	0.354	0.317	0.336	0.387
Set CMS Subset 1	0.361	0.340	0.347	0.364
Set CMS Subset 2	0.560	0.484	0.431	0.459
Set CMS Subset 3	0.431	0.397	0.331	0.357
Set CMS Subset 4	0.327	0.301	0.347	0.356
Set CMS Subset 5	0.367	0.342	0.346	0.356

Max Abut Disp: maximum abutment displacement in the unseating direction
ZL-1: zero-length element left abutment
ZL-2: zero-length element right abutment

Table 3.3.1b. Bridge A. Max Abut Disp/Gap Size. Unidirectional Studies

	ZL-1 TOP	ZL-1 BOTTOM	ZL-2 TOP	ZL-2 BOTTOM
Set Sa(T_1)	0.364	0.357	0.405	0.413
Set CMS Subset 1	0.382	0.374	0.385	0.393
Set CMS Subset 2	0.446	0.433	0.314	0.321
Set CMS Subset 3	0.378	0.365	0.354	0.365
Set CMS Subset 4	0.502	0.479	0.300	0.312
Set CMS Subset 5	0.380	0.372	0.356	0.369

Max Abut Disp: maximum abutment displacement in the unseating direction
ZL-1: zero-length element left abutment
ZL-2: zero-length element right abutment

Table 3.3.2a. Bridge A. Maximum Bent Drift Ratio (%). Bidirectional Studies

	Set Sa(T_1)	Set CMS Subset 1	Set CMS Subset 2	Set CMS Subset 3	Set CMS Subset 4	Set CMS Subset 5
Bent 1	2.1	2.0	2.3	2.0	1.9	2.0

Table 3.3.2b. Bridge A. Maximum Bent Drift Ratio (%). Unidirectional Studies

	Set Sa(T_1)	Set CMS Subset 1	Set CMS Subset 2	Set CMS Subset 3	Set CMS Subset 4	Set CMS Subset 5
Bent 1	1.9	1.8	1.9	1.7	2.1	1.7

BRIDGE B

Table 3.4.1a. Bridge B. Max Abut Disp/Gap Size. Bidirectional Studies

	ZL-1 TOP	ZL-1 BOTTOM	ZL-2 TOP	ZL-2 BOTTOM
Set Sa(T_1)	0.398	0.407	0.408	0.400
Set CMS Subset 1	0.407	0.402	0.396	0.398
Set CMS Subset 2	0.482	0.479	0.533	0.520
Set CMS Subset 3	0.494	0.497	0.379	0.378
Set CMS Subset 4	0.407	0.402	0.396	0.401
Set CMS Subset 5	0.431	0.421	0.383	0.394

Max Abut Disp: maximum abutment displacement in the unseating direction
ZL-1: zero-length element left abutment
ZL-2: zero-length element right abutment

Table 3.4.1b. Bridge B. Max Abut Disp/Gap Size. Unidirectional Studies

	ZL-1 TOP	ZL-1 BOTTOM	ZL-2 TOP	ZL-2 BOTTOM
Set Sa(T_1)	0.441	0.441	0.457	0.457
Set CMS Subset 1	0.513	0.513	0.555	0.555
Set CMS Subset 2	0.530	0.530	0.527	0.527
Set CMS Subset 3	0.420	0.420	0.419	0.419
Set CMS Subset 4	0.448	0.448	0.452	0.452
Set CMS Subset 5	0.435	0.435	0.472	0.472

Max Abut Disp: maximum abutment displacement in the unseating direction
ZL-1: zero-length element left abutment
ZL-2: zero-length element right abutment

Table 3.4.2a. Bridge B. Maximum Bent Drift Ratio (%). Bidirectional Studies

	Set Sa(T_1)	Set CMS Subset 1	Set CMS Subset 2	Set CMS Subset 3	Set CMS Subset 4	Set CMS Subset 5
Bent 1	2.9	2.6	3.0	2.6	2.6	2.5

Table 3.4.2b. Bridge B. Maximum Bent Drift Ratio (%). Unidirectional Studies

	Set Sa(T_1)	Set CMS Subset 1	Set CMS Subset 2	Set CMS Subset 3	Set CMS Subset 4	Set CMS Subset 5
Bent 1	2.3	2.3	2.3	1.7	2.2	2.1

BRIDGE C

Table 3.5.1a. Bridge C. Max Abut Disp/Gap Size. Bidirectional Studies

	ZL-1 TOP	ZL-1 BOTTOM	ZL-2 TOP	ZL-2 BOTTOM
Set Sa(T_1)	0.761	0.507	0.493	0.665
Set CMS Subset 1	0.904	0.549	0.153	0.594
Set CMS Subset 2	0.703	0.617	0.658	0.772
Set CMS Subset 3	0.593	0.467	0.653	0.885
Set CMS Subset 4	0.656	0.477	0.562	0.809
Set CMS Subset 5	0.577	0.443	0.569	0.710

Max Abut Disp: maximum abutment displacement in the unseating direction
ZL-1: zero-length element left abutment
ZL-2: zero-length element right abutment

Table 3.5.1b. Bridge C. Max Abut Disp/Gap Size. Unidirectional Studies

	ZL-1 TOP	ZL-1 BOTTOM	ZL-2 TOP	ZL-2 BOTTOM
Set Sa(T_1)	0.645	0.598	0.584	0.623
Set CMS Subset 1	0.584	0.523	0.596	0.652
Set CMS Subset 2	0.663	0.602	0.629	0.687
Set CMS Subset 3	0.428	0.364	0.669	0.784
Set CMS Subset 4	0.553	0.498	0.557	0.591
Set CMS Subset 5	0.522	0.495	0.611	0.665

Max Abut Disp: maximum abutment displacement in the unseating direction
ZL-1: zero-length element left abutment
ZL-2: zero-length element right abutment

Table 3.5.2a. Bridge C. Maximum Bent Drift Ratio (%). Bidirectional Studies

	Set Sa(T_1)	Set CMS Subset 1	Set CMS Subset 2	Set CMS Subset 3	Set CMS Subset 4	Set CMS Subset 5
Bent 1	3.5	3.2	2.6	3.5	3.7	3.4
Bent 2	3.3	3.8	2.8	3.1	3.0	3.4

Table 3.5.2b. Bridge C. Maximum Bent Drift Ratio (%). Unidirectional Studies

	Set Sa(T_1)	Set CMS Subset 1	Set CMS Subset 2	Set CMS Subset 3	Set CMS Subset 4	Set CMS Subset 5
Bent 1	2.7	2.7	2.5	2.8	2.3	2.4
Bent 2	2.7	2.7	2.5	2.8	2.3	2.4

BRIDGE D

Table 3.6.1a. Bridge D. Max Abut Disp/Gap Size. Bidirectional Studies

	ZL-1 TOP	ZL-1 BOTTOM	ZL-2 TOP	ZL-2 BOTTOM
Set Sa(T_1)	0.406	0.424	0.406	0.514
Set CMS Subset 1	0.365	0.399	0.365	0.477
Set CMS Subset 2	0.358	0.359	0.338	0.498
Set CMS Subset 3	0.318	0.341	0.309	0.383
Set CMS Subset 4	0.363	0.427	0.250	0.405
Set CMS Subset 5	0.324	0.354	0.318	0.399

Max Abut Disp: maximum abutment displacement in the unseating direction
ZL-1: zero-length element left abutment
ZL-2: zero-length element right abutment

Table 3.6.1b. Bridge D. Max Abut Disp/Gap Size. Unidirectional Studies

	ZL-1 TOP	ZL-1 BOTTOM	ZL-2 TOP	ZL-2 BOTTOM
Set Sa(T_1)	0.361	0.385	0.260	0.363
Set CMS Subset 1	0.331	0.370	0.245	0.329
Set CMS Subset 2	0.364	0.352	0.241	0.326
Set CMS Subset 3	0.305	0.319	0.208	0.285
Set CMS Subset 4	0.313	0.345	0.213	0.279
Set CMS Subset 5	0.303	0.331	0.214	0.298

Max Abut Disp: maximum abutment displacement in the unseating direction
ZL-1: zero-length element left abutment
ZL-2: zero-length element right abutment

Table 3.6.2a. Bridge D. Maximum Bent Drift Ratio (%). Bidirectional Studies

	Set Sa(T_1)	Set CMS Subset 1	Set CMS Subset 2	Set CMS Subset 3	Set CMS Subset 4	Set CMS Subset 5
Bent 1	1.9	1.6	1.8	1.5	1.6	1.6

Table 3.6.2b. Bridge D. Maximum Bent Drift Ratio (%). Unidirectional Studies

	Set Sa(T_1)	Set CMS Subset 1	Set CMS Subset 2	Set CMS Subset 3	Set CMS Subset 4	Set CMS Subset 5
Bent 1	1.5	1.4	1.4	1.3	1.3	1.2

BRIDGE E

Table 3.7.1a. Bridge E. Max Abut Disp/Gap Size. Bidirectional Studies

	ZL-1 TOP	ZL-1 BOTTOM	ZL-2 TOP	ZL-2 BOTTOM
Set Sa(T_1)	0.519	0.479	0.518	0.490
Set CMS Subset 1	0.412	0.406	0.519	0.442
Set CMS Subset 2	0.533	0.513	0.553	0.539
Set CMS Subset 3	0.447	0.489	0.477	0.432
Set CMS Subset 4	0.527	0.470	0.463	0.467
Set CMS Subset 5	0.491	0.469	0.503	0.454

Max Abut Disp: maximum abutment displacement in the unseating direction
ZL-1: zero-length element left abutment
ZL-2: zero-length element right abutment

Table 3.7.1b. Bridge E. Max Abut Disp/Gap Size. Unidirectional Studies

	ZL-1 TOP	ZL-1 BOTTOM	ZL-2 TOP	ZL-2 BOTTOM
Set Sa(T_1)	0.478	0.470	0.379	0.404
Set CMS Subset 1	0.498	0.491	0.341	0.379
Set CMS Subset 2	0.443	0.435	0.321	0.358
Set CMS Subset 3	0.481	0.479	0.422	0.429
Set CMS Subset 4	0.576	0.560	0.409	0.470
Set CMS Subset 5	0.470	0.463	0.377	0.403

Max Abut Disp: maximum abutment displacement in the unseating direction
ZL-1: zero-length element left abutment
ZL-2: zero-length element right abutment

Table 3.7.2a. Bridge E. Maximum Bent Drift Ratio (%). Bidirectional Studies

	Set Sa(T_1)	Set CMS Subset 1	Set CMS Subset 2	Set CMS Subset 3	Set CMS Subset 4	Set CMS Subset 5
Bent 1	1.8	1.5	1.5	1.6	1.9	1.8
Bent 2	1.8	1.6	1.5	1.7	2.0	1.8

Table 3.7.2b. Bridge E. Maximum Bent Drift Ratio (%). Unidirectional Studies

	Set Sa(T_1)	Set CMS Subset 1	Set CMS Subset 2	Set CMS Subset 3	Set CMS Subset 4	Set CMS Subset 5
Bent 1	1.3	1.3	1.2	1.3	1.5	1.3
Bent 2	1.2	1.2	1.1	1.1	1.3	1.1

The results are identified as: SetSa result (SetSa result stands for the median of the EDP obtained applying the set of ground motion records selected and modified according to Sa scaling method) and SetCMSSubset*i* result (SetCMSSubset*i* result stands for the median of the EDP obtained applying the i^{th} subset of ground motion records selected and modified according to CMS scaling method). For each EDP (EDP1 and EP2), the following is observed:

- EDP1
    - For bridges A and B and both bidirectional and unidirectional ground motion studies, SetSa results are similar to SetCMSSubset5 results, but not to SetCMSSubset1, SetCMSSubset2, SetCMSSubset3 and SetCMSSubset4 results. For the rest of the bridges, none of the results are similar to the others.
    - For Bridge B and unidirectional studies, the values of ZL-*i* TOP and ZL-*i* BOTTOM (for $i = 1$ and $i = 2$) are the same, which proves that Bridge B, with skew angle equal to 0º, does not rotate. However, for bridges A and C, the values of ZL-*i* TOP and ZL-*i* BOTTOM (for $i = 1$ and $i = 2$) are not the same. This results evidence the fact that skew angles different than 0º makes bridge decks rotate.
    - For Bridge D, SetSa results are larger than SetCMSSubset*i* results. However, this trend does not happen with the rest of the bridges.
- EDP2
    - For all bridges, SetSa results are similar to SetCMSSubset1, SetCMSSubset12, SetCMSSubset3, SetCMSSubset4 and SetCMSSubset5 results. The maximum difference between the results is no larger than 0.5%.

CHAPTER 5

FINDINGS, CONCLUSIONS AND FUTURE WORK

The present thesis depicts the research work conducted for evaluating two GMSM methods selected because of being commonly used and also because of the consistency of the theoretical principles in which they are based. To accomplish this purpose, the following steps are followed. Firstly, a group of structures, six bridges in this case, is chosen and modeled. The second step consists in defining a target ground motion scenario and, according to it, generating a large bin of ground motion records. The next step is to use the GMSM methods to select and modify sets of records from the same bin. These sets of ground motions are then applied to the bridges and predictions of their structural responses are obtained. Finally, such predictions are compared and contrast.

The selected GMSM methods are the $Sa(T_1)$ scaling method and the CMS scaling method. Six bridges, representative of a wide range of typologies commonly used, have been modeled using OpenSees open-source structural analysis platform. The ground motion scenario is defined by an M 7.0 earthquake occurring on a strike-slip fault, a source-to-site distance of 10 km, and a soil with a shear wave velocity for the top 30 m ($V_{S,30}$) of its profile equal to 400 m/s. According to this target ground motion scenario, a bin of one hundred and seventeen ground motion records is generated.

This study pays special attention not only to the evaluation of the aforementioned selected GMSM methods, but also to the modeling and behavior of the six bridges, identified as bridges A, B, C, D, E and F. Bridge A is two-span straight bridge; bridges B

and C are skewed bridges with two and three spans, respectively; bridges D, E and F are curved bridges, with one, two and three spans. They have been designed by the California Transportation Department, Caltrans, and are located in Los Angeles and Orange counties. According to SDC 2006, Section 1.1, they are classified as ordinary standard bridges.

5.1. FINDINGS

The first aspect observed is the ability of *Concrete07* model, which is a material model available in OpenSees, to derive the compressive strength of confined concrete from the compressive strength of the unconfined concrete and a given value of the confinement pressure of the cross section of the element being modeled. Although the material model used is *Concrete01*, *Concrete07* is likely to be used in future studies because of its apparently accurate representation of confined concrete behavior.

The second aspect observed is the impossibility to assign effective properties to those elements modeled in the fiber section. Also related to effective properties, it is important to be aware of the significant reduction of the torsion stiffness that must be taken into consideration for columns. A reduction of the 80% of such stiffness has been considered herein.

Another remark to be mentioned is the difficultness of properly model the abutments of skewed bridges. Efforts are currently being done by the engineering research community to address the weaknesses of the models being used nowadays.

The foundations of curved bridges' columns are modeled by translational and rotational springs. For Bridge F, theses springs interact, i.e., the off-diagonal terms of the

stiffness matrix of such foundations cannot be assumed to be zero. Springs are modeled in OpenSees using zero-length elements. However, these elements can only model uncoupled springs, and there is not any specific available finite element that can model coupled springs. A solution consisting in a cantilever column with certain properties is proposed to model the foundations of Bridge F's columns. This solution is the first finding exposed herein.

Another finding is that displacement-based elements, used for columns, have shown better numerical stability compared to force-based elements, as expected. Displacement-based are the elements finally used for modeling the columns.

It has also been found that, given a bridge, conducting pushover analysis of the structure at every 5º is likely to be a potentially satisfactory strategy to identify its strongest and weakest directions, which can be related to longitudinal and transverse directions. This method can also be used to determine the fundamental period of the structure accounting for the effective properties of the columns when their cross section is modeled using a fiber section model.

Finally, an extremely simple model to record the accelerations that OpenSees inputs to a model when this is applied a certain ground motion record has been created, and a methodology to determine the plastic hinge length of the columns has been proposed and tested.

5.2. CONCLUSIONS

Along with the modeling of the structures, side studies have been conducted for different purposes. Some of the conclusions refer to modeling issues strictly, and others to the

behavior of skewed and curved bridges derived from the analysis of the performance of the models of such structures. The conclusions derived from the evaluation of Sa scaling and CMS scaling GMSM methods are also exposed.

Curved bridges have presented numerical instabilities when using force-based elements to model the columns, so displacement-based elements have been used instead. The optimal solution in order to have an accurate response using these elements consists in using five elements per column and five integration points per element.

Pushover analysis of the bridges have been conducted every 5º. The results show that the strongest direction of curved bridges is the direction parallel to an axis approximately tangent to the arc defined by the deck in its middle point. For the straight Bridge B, this direction is associated to the longitudinal axis, as expected. However, for skewed bridges A and C, the strongest direction is the transverse direction. For these last structures, it was expected the longitudinal direction to be the strongest. Such unexpected response may be due to an overestimation of the capacity of the shear keys.

In order to record the accelerations that OpenSees inputs to a model, given a certain ground motion, the following model has been created: an infinitely rigid cantilever column, with unit mass and unit length. Recording the base shear of this model is equivalent to record such accelerations. Using this model, it has been shown that OpenSees makes linear interpolation to determine those ground motion accelerations for which no value is specified. It can also be shown that if the maximum time of the dynamic analysis is larger than that of the ground motion record, OpenSees considers null acceleration for those times that are beyond the maximum time of the record.

A procedure to determine the plastic hinge length of a column has been proposed. It consists in (1) determine the time history of axial force and bending moment values at the integration points of all the elements used to model the column, (2) for each axial force, compute the corresponding plastic moment capacity, and (3) compare the bending moment and the plastic moment capacity to determine which integration points reach such capacity during the ground motion. These points will define the plastic hinge length, and their location is given by the quadrature rule used by the finite elements with which the column is modeled. The procedure results to be consistent. However, progress must be done to reduce the time involved in each realization of the procedure, in order to be able to use it in analyzes where many ground motions are considered.

Finally, the Sa scaling and CMS scaling methods have been evaluated. The median values of the selected EDPs, obtained applying to the structures the sets of ground motion records selected and modified using these two methods, show no clear trend, thus it is not possible to reach a conclusion regarding the suitability of such methods for capturing a reliable structural response of the bridges.

5.3. FUTURE WORK

Firstly, an Inelastic method, which is another type GMSM method, should also be evaluated. Inelastic methods select ground motions by using two possible criteria. The first criterion in to select ground motions such that their properties related to inelastic spectral displacement are as close as possible to corresponding properties derived from the target ground motion scenario. The second criterion consists of selecting ground

motions by applying the first criterion and also considering how well the scaled ground motion fits the CMS at the second-mode period of the structure.

After evaluating this additional GMSM method, two POCs should be created, one for unidirectional ground motion studies and another for bidirectional ground motion studies, and the responses predicted by Sa scaling, CMS scaling and Inelastic methods should be compared to them in order to have a more complete and accurate evaluation of such methods. Developing practical guidelines for the use of GMS methods in bridge design should be the following step.

The procedure to determine the plastic hinge length exposed in Chapter 3 is waiting to be optimized. Its optimization is of capital importance for conducting future studies that will aim for defining accurate formulations to predict the plastic hinge length.

Lastly, it is important to keep conducting side studies to clarify all kind of uncertainties associated with modeling issues. The bridges considered in this study have been modeled using OpenSees open-source structural analysis platform. Such platform is under development. Side studies can also be used to identify modeling aspects that cannot currently be addressed by OpenSees, such as coupled orthogonal springs or material models being able to die in compression, as explained in Chapter 3. Therefore, they can also be used to justify and propose modifications of such platform.

BIBLIOGRAPHY

Mander, J.B., Priestley, M.J.N., Park R. (1988). Theoretical Stress – Strain Model for Confined Concrete. *Journal of Structural Engineering – ASCE*. **114:8**,1804-1826.

Neuenhofer, A. and Filippou, F.C. (1997). Evaluation of Nonlinear Frame Finite-Element Models. *Journal of Structural Engineering – ASCE*. **123:7.**958-966.

Neuenhofer, A. and Filippou, F.C. (1998). Geometrically Flexibility-Based Frame Finite Element. *Journal of Structural Engineering – ASCE*. **124:6.**704-711.

McKenna, F., Fenves, G.L. and Scott, M.H. (2000), Open System for Earthquake Engineering Simulation, University of California Berkeley, California, http://opensees.berkeley.edu.

Alemdar, B.N. and White, D.W. (2005). Displacement, Flexibility, and Mixed Beam-Column Finite Element Formulations for Distributed Plasticity Analysis. *Journal of Structural Engineering – ASCE*. **131:12** 1811-1819.

Caltrans SDC. (2006). Caltrans Seismic Design Criteria Version 1.4. California Department of Transportation.

Manterola, J. (2006), Puentes. Apuntes para su Diseño, Cálculo y Construcción, CICCP (Colección Escuelas).

Aviram A ac kie and toj adinovi , B. (2008). Guidelines for Nonlinear Analysis of Bridge Structures in California. PEER Report 2008/3, Pacific Earthquake Engineering Research Center. College of Engineering, University of California, Berkeley.

Waugh, J., Aaleti, S., Sritharan, S., Zhao, J. (2008). Nonlinear Analysis of Rectangular and T-Shaped Concrete Walls. ISU – ERI – Ames Report ERI – 09327. Department of Civil, Construction and Environmental Engineering, Iowa State University.

Federal Emergency Management Agency (FEMA). (2009). Recommended Methodology for Quantification of Building System Performance and Response Parameters. FEMA P695 (ATC-63 Project), Prepared for the Federal Emergency Management Agency, Prepared by the Applied Technology Council, Redwood City, CA.

PEER GMSM, Haselton, C.B., Editor (2009). Evaluation of Ground Motion Selection and Modification Methods: Predicting Median Interstory Drift Response of Buildings. PEER Report 2009/01, Pacific Engineering Research Center, University of California, Berkeley, California.

Baker, J.W. (2010). The Conditional Mean Spectrum: A tool for ground motion selection. *Journal of Structural Engineering – ASCE (in press)*.

Jayaram, N., Lin, Lin, T., Baker, W. (2010). A Computationally Efficient Ground-Motion Selection Algorithm for Matching a Target Response Spectrum Mean and Variance. Department of Civil and Environmental Engineering, Stanford, CA.

PEER. (2010). Pacific Earthquake Engineering Research Center: PEER NGA Database, University of California, Berkeley, http://peer.berkeley.edu/nga/ (last accessed May, 2010).

APPENDIX A

MODELS FOR BRIDGES D, E AND F FOUNDATIONS

This appendix describes the modeling of the foundations of bridges D, E and F. T. Shantz, Senior Research Engineer from Caltrans Division of Research and Innovation, was responsible for this modeling. The models consist in a series of springs that approximate the behavior of the foundations.

The following is the input information he was provided with in order to conduct the modeling in question. At the end, the results he obtained from his models and his explanations about the process he followed and the assumptions he made to develop such models are also exposed.

MAXIMUM COLUMN AXIAL FORCE

The determination of the maximum column axial force needed for modeling the foundations of bridges D, E and F is based on the loads and combinations of the same specified in AASHTO LRDF Bridge Design Specifications, 4th Edition, 2007.

Combinations of loads associated with the limit state Extreme Event I are the combinations considered to determine the maximum column axial force associated to dead and live loads. The following is the explanation of the loads considered and their combination. The maximum column axial forces obtained applying such combinations are also exposed, as well as other input information needed for the modeling.

Limit state Extreme Event I

Load combination including earthquake. The total factored force effect is taken as:

$$= \sum_{i\ i\ i}$$

where:

$_i$ = load modifier, equal to 1.00 for the limit state Extreme Event I

$_i$ = load factors specified in next table

$_i$ = force effects from loads specified above

Load combinations and load factors:

Table A.1. Load combinations and load factors

Load Combination Limit State	DC DD DW EH EV ES EL	LL IM CE BR PL LS	WA	WS	WL	FR	TU CR SH	TG	SE	Use One of These at a Time			
										EQ	IC	CT	CV
EXTREME EVENT I	$_p$	EQ	1.00	_	_	1.00	_	_	_	1.00	_	_	_

For DC $_{pmax}$ = a nd $_{pmin}$ = 0.90.

Permanent loads:

- DD = downdrag
- DC = dead load of structural components and nonstructural attachments
- DW = dead load of wearing surfaces and utilities
- EH = horizontal earth pressure load
- EV = accumulated locked-in force effects resulting from the construction process, including the secondary forces from post-tensioning
- ES = earth surcharge load
- EL = vertical pressure from dead load of earth fill

Transient loads:

- LL = vehicular live load
- IM = vehicular dynamic load allowance
- CE = vehicular centrifugal force
- BR = vehicular braking force
- PL = pedestrian live load
- LS = live load surcharge
- WA = water load and stream pressure
- WS = wind load on structure
- WL = wind on live load
- FR = friction
- TU = uniform temperature
- CR = creep
- SH = shrinkage
- TG = temperature gradient
- SE = settlement
- EQ = earthquake
- IC = ice load
- CT = vehicular collision force
- CV = vessel collision force

The dead and live loads considered are those in red color, i.e.: dead loads: DC; live loads: LL, IM.

In the application of the permanent loads, it is unnecessary to assume that one type of load varies by span, length, or component within a bridge.

he possibility of partial live load i e $_{EQ} < 1.0$, with earthquakes is the situation here considered Application of urkst ra's rule for combining uncorrelated loads indicates that $_{EQ} = 0.5$ is reasonable for a wide range of values of average daily truck traffic (ADTT). Therefore, this is the value applied to the live loads acting simultaneously with the earthquake.

Dead Loads: DD

Dead load includes the weight of the structural components and non-structural attachments. It is considered there are not wearing surfaces neither utilities. It is also considered drawndag is not developed.

Live Loads

Vehicular Live Load: LL

For the maximum axial force in the columns, both lanes are considered to be loaded, which implies the multiple presence factors to be equal to 1.20, if only one lane is loaded, and equal to 1.00 if both lanes are laded. The vehicular live loading consists of a combination of the:

- Design truck or design tandem, and
- Design lane load.

The design truck is idealized as a punctual force equal to 325kN, while the design tandem, as a punctual force equal to 220kN. The design lane load consists of a load of

9.3kN/m uniformly distributed in the longitudinal direction. Unlike the design truck or design tandem, the force effects from the design lane load are not subjected to a dynamic load allowance.

The extreme force effect is taken as the larger of the following:

- The effect of the design tandem combined with the effect of the design lane load, or
- The effect of one design truck combined with the effect of the design lane load.

The effects of an axle sequence and the lane load are superposed in order to obtain extreme values.

The lane load is not interrupted to provide space for the axle sequences of the design tandem or the design truck.

Since the goal is to obtain the maximum reaction at columns, only the 90 percent of the effect of two design trucks combined with 90 percent of the effect of the design lane load is considered.

Dynamic Load Allowance: IM

The static effects of the design truck or tandem are increased by 33%.

Combinations of Loads for Maximum Column Axial Force

Curved Bridge D

Column 2 Span 1 and Span 2 loaded with twice the design lane load and column 2 loaded with twice the design truck.

Curved Bridge E

Column 2 Span 1 and Span 2 loaded with twice the design lane load and column 2 loaded with twice the design truck.

Column 3 Span 2 and Span 3 loaded with twice the design lane load and column 3 loaded with twice the design truck.

Curved Bridge F

Column 2 Span 1 and Span 2 loaded with twice the design lane load and column 2 loaded with twice the design truck.

Column 3 Span 2 and Span 3 loaded with twice the design lane load and column 3 loaded with twice the design truck.

Column 4 Span 3 and Span 4 loaded with twice the design lane load and column 4 loaded with twice the design truck.

Resulting Axial Loads. Curved Bridge D

Applying all modifications factors specified in AASHTO 2007:

Table A.2a. Axial Loads. Curved Bridge D (I)

	Dead + Live loads (Not considering column self-weight)		**Column self-weight**	
	kN	**kips**	**kN**	**Kips**
Column 2	7282.64	1637.20	443.406	99.6817

Considering all modification factors equal to 1.00:

Table A.2b. Axial Loads. Curved Bridge D (II)

	Dead + Live loads (Not considering column self-weight)		**Column self-weight**	
	kN	**kips**	**kN**	**Kips**
Column 2	6760.05	1519.72	354.725	79.7454

Considering all modification factors equal to 1.00 and no amplification of the design truck due to dynamic effects:

Table A.2c. Axial Loads. Curved Bridge D (III)

	Dead + Live loads (Not considering column self-weight)		**Column self-weight**	
	kN	**kips**	**kN**	**Kips**
Column 2	6545.98	1471.59	354.725	79.7454

More information: Column 2 diameter: 5.51ft; % of steel of the column 2: 2%.

Resulting Axial Loads. Curved Bridge E

Applying all the modifications factors specified in AASHTO 2007:

Table A.3a. Axial Loads. Curved Bridge E (I)

	Dead + Live loads (Not considering column self-weight)		**Column self-weight**	
	kN	**kips**	**kN**	**Kips**
Column 2	14010.4	3149.66	1802.90	405.308
Column 3	14075.3	3164.25	1853.45	416.672

Considering all the modification factors equal to 1.00:

Table A.3b. Axial Loads. Curved Bridge E (II)

	Dead + Live loads (Not considering column self-weight)		**Column self-weight**	
	kN	**kips**	**kN**	**Kips**
Column 2	12499.0	2809.89	1442.32	324.247
Column 3	12553.9	2822.23	1482.76	333.338

Considering all the modification factors equal to 1.00 and no amplification of the design truck due to dynamic effects:

Table A.3c. Axial Loads. Curved Bridge E (III)

	Dead + Live loads (Not considering column self-weight)		**Column self-weight**	
	kN	**kips**	**kN**	**Kips**
Column 2	12284.6	2761.69	1442.32	324.247
Column 3	12339.5	2774.03	1482.76	333.338

More information: Column 2 diameter: 8.99ft; % of steel of the column 2: 2.8%; Column 3 diameter: 8.99ft; % of steel of the column 3: 2.8%.

Resulting Axial Loads. Curved Bridge F

Applying all modifications factors specified in AASHTO 2007:

Table A.4a. Axial Loads. Curved Bridge F (I)

	Dead + Live loads (Not considering column self-weight)		**Column self-weight**	
	kN	**kips**	**kN**	**Kips**
Column 2	11638.5	2616.44	870.978	195.804
Column 3	13580.1	3052.93	762.105	171.328
Column 4	12588.2	2829.94	702.720	157.978

Considering the modification factors equal to 1.00:

Table A.4b. Axial Loads. Curved Bridge F (II)

	Dead + Live loads (Not considering column self-weight)		**Column self-weight**	
	kN	**kips**	**kN**	**Kips**
Column 2	10505.4	2361.71	696.782	156.643
Column 3	12153.4	2732.19	609.684	137.062
Column 4	11296.7	2539.60	562.176	126.382

Considering the modification factors equal to 1.00 and no amplification of the design truck due to dynamic effects:

Table A.4c. Axial Loads. Curved Bridge F (III)

	Dead + Live loads (Not considering column self-weight)		**Column self-weight**	
	kN	**kips**	**kN**	**Kips**
Column 2	10291.3	2313.58	696.782	156.643
Column 3	11939.3	2684.06	609.684	137.062
Column 4	11082.9	2491.54	562.176	126.382

More information: Column 2 diameter: 6.89ft; % of steel of the column 2: 1.3%; Column 3 diameter: 6.89ft; % of steel of the column 3: 1.4%**;** Column 4 diameter: 6.89ft**;** % of steel of the column 4: 2.3%.

FOUNDATION MODELING

The models of the foundations consist in a series of elastic springs reproducing the behavior of this part of the structure. The stiffnesses of these springs, i.e., the models of the foundations, were computed by T. Shantz. The following is an almost exact reproduction of the document he generate with explanations related to the modeling of the springs and the results he obtained.

The author of the present project has modified the text slightly. The way of identifying the bridges has been changed and two figures have been omitted. No more changes have been done.

Foundation Stiffnessess for Curved Bridges D, E and F

For bridges D and E the same pile type was used. All bridges used the same soil profile. The Class 625 pile is a metric designation for what traditionally was referred to as Class 70 pile. This is a widely used pile, typically precast/prestressed concrete, 14 in x 14 in or in dia he " " means capable of supplying tons capacity for design load ince a factor of safety of 2 is used, the ultimate capacity of this pile in compression is 280 kips at 0.5 in deflection. In uplift, half the capacity is assumed (140 kips at 0.5 in). For determination of rotational stiffness, each pile was modeled with a load deformation behavior following the above criteria.

In the determination of the rotational stiffness, the pile cap was assumed to be rigid and the top of the piles were assumed to be pinned into the pile cap.

For the determination of the lateral stiffness, a soil profile, pile diameter, and pile stiffness had to be assumed. The soil profile used was based on one developed by Ketchum et al. (2004). This profile was the product of an evaluation of typical profiles for a given pile type. The idea was to recognize that a bridge with H-piles will typically have a much stiffer soil profile (since H-piles are used for hard driving conditions) than bridges using steel pipe piles (typically sites with soft soil conditions). Bridges using precast concrete piles are typically not too stiff or not too soft. However, one should recognize that variability from site to site is quite high, even when controlling for pile type. So there no correct answers, only reasonable ones.

The assumed pile diameter was 15 in and the pile stiffness (EI) was assumed to be $4 \cdot 10^6$ kip-in. Finally, for bridges D and E, since the pile to pile cap connection is pinned, the off-diagonal terms in the stiffness matrix are relatively small relative to the overall

uncertainty of the diagonal terms. Furthermore, both foundations are approximately symmetric. Thus, the stiffness matrix is characterized by only two terms: K_θ and K_H. The results are as follows:

- Bridge D: $K_\theta = 1.8 \cdot 10^8$ kip-in/rad

  $K_H = 300$ kip/in

- Bridge E: $K_\theta = 5.0 \cdot 10^8$ kip-in/rad

  $K_H = 830$ kip/in

For Bridge F, the foundation is a 6.9 ft diameter drilled shaft. A stiffness (EI) of $3 \cdot 10^9$ kip-in^2 was assumed. Since there is a large interaction between deflection, moment and rotation in the shaft, off-diagonal stiffness terms are supplied as well. The results are as follows:

$K_\theta = 3.6 \cdot 10^7$ kip-in/rad

$K_H = 1275$ kips/in

$K_{\theta H} = K_{H\theta} = -179000$ kips